Supplementary Information

Large and Long-Term Photon Energy Storage in Diazetidines *via* [2+2] Photocycloaddition

Han P. Q. Nguyen, Anurag Mukherjee, Junichi Usuba, Joshua Wan, and Grace G. D. Han*

Department of Chemistry, Brandeis University, 415 South Street, Waltham, MA 02453, USA

E-mail: gracehan@brandeis.edu

Table of Contents

1. Material and methods 3
   a. General methods 3
   b. Differential scanning calorimetry (DSC) 3
   c. Thermal reversion kinetics measurement by DSC 4
   d. UV-vis absorption spectroscopy in solutions 5
   e. Thermal reversion kinetics measurement in solutions by UV-vis spectroscopy 5
   f. Cycling test 6
   g. Computational methods 6
2. UV-vis absorption spectroscopy in solution 7
3. Synthesis procedures of monomers and dimers 8
4. NMR and FT-IR characterization of PBs and DAs 9
5. Differential scanning calorimetry (DSC) 31
6. Cycling test 32
7. Isothermal DSC 33
8. Thermal reversion kinetics measurement by DSC 34
9. Evaluation of solvation energy 36
10. Thermogravimetric analysis (TGA) 37
11. DSC of dimer in solution 38
12. ^{1}H NMR spectra of dimers after DSC measurement 39
13. Thermal reversion kinetics measurement in solutions by UV-vis spectroscopy 43
14. Computational studies: Thermal cycloreversion 47
15. Comparison of reported cycloaddition MOST systems 51
16. Computational studies: Dearomative cycloaddition 51
17. References 59

1. Material and methods

a. General methods

Commercial sources provided all reagents and initial materials, which were used as received unless specified otherwise. Deuterated solvents were acquired from Cambridge Isotope Laboratories, Inc. and were utilized without any modifications. ^{1}H, ^{13}C, and ^{19}F NMR spectra were collected using an AVANCE NEO 400 NMR, operating at frequencies of 400 MHz for ^{1}H NMR, 100 MHz for ^{13}C NMR, and 565 MHz for ^{19}F NMR. Chemical shifts are expressed in parts per million (ppm) with respect to tetramethylsilane (TMS), employing the solvent's residual peak as a secondary reference. Photo irradiation experiments were performed using LED from Thorlabs, Inc., model M300L4 (300 nm, 0.3 μW/mm^2, 2275 mW), and Rayonet photoreactor from Southern New England Ultraviolet Company, model RPR-100 (300 nm, 32 μW/cm^2, 35 000 mW). FT-IR spectra were recorded in a Nicolet IR200 spectrometer equipped with an Everest™ Diamond ATR accessory. The PXRD patterns were obtained using a Rigaku MiniFlex600 diffractometer with a CuKα source (λ = 1.5405 Å).

b. Differential scanning calorimetry (DSC)

DSC analysis was conducted using a DSC 250 instrument from TA Instruments, which was equipped with an RSC 90 cooling component. For solid-state measurements, the samples were initially heated to a temperature range of 20-160 °C, then cooled down to −20 °C at a rate of 2 °C/min. In the solvated-solid analysis, suspensions of dimer samples (0.5-0.7 mg) in toluene (25 μL) were initially heated to a temperature range of 20-100 °C, then cooled down to −20 °C at the same rate. The solvation energy of PB was investigated by heating suspensions of PB samples (0.9 and 2.3 mg) in toluene (25 μL) across the same temperature range (20-100 °C).

c. Thermal reversion kinetics measurement by DSC

Thermal DA→2PB reversion kinetics were determined using established isothermal DSC methods. Under isothermal conditions, the degree of an exothermic reaction is directly proportional to the amount of heat evolved.

$$\alpha_i = \frac{\sum \Delta H_i}{\Delta H_{rxn}} \qquad \text{(Equation 1)}$$

i indicates incremental measurements, *α* indicates fractional conversion or extent of the reaction, ΔH_i indicates partial heat generated, and ΔH_{rxn} indicates the total heat of the reaction.

In isothermal DSC, partial heat ΔH_i is obtained from the area under the exothermic peak.

$$\Delta H_i = \int_0^i \frac{dH}{dt} dt \qquad \text{(Equation 2)}$$

dH/*dt* indicates heat flow, and *t* is time in seconds.

DAs **1**-**4** (3.13 ± 0.02 mg) was hermetically sealed in an aluminum pan. The DSC cell was pre-heated to the target isothermal temperature and stabilized for at least 5 minutes. The DA sample was then quickly loaded into the cell, and data collection was immediately initiated. In the case of DA-**3**, the DSC cell was pre-heated to 100 °C, the highest standby temperature available for this instrument. After loading the sample and initiating the data collection, the sample was quickly ramped to the target isothermal temperature, and the isothermal experiment proceeded. The reversion of DAs **1**-**4** was monitored at three different isothermal temperatures.

From the isothermal DSC curve, heat flow *dH*/*dt* was obtained as a function of time then integrated to calculate the partial heat ΔH_i (Equation 2). The total heat ΔH_{rxn} was derived from the total heat integrated from the isothermal DSC curve. Subsequently, fractional conversion α of each compound at three different temperatures was calculated using Equation 1.

An exponential fit of fractional conversion *α* as a function of time was performed to determine the experimental rate constant *k* of the reversion. The Gibbs free energy of activation $\Delta G^{\ddagger}$ of the reversion was determined from the Eyring plot of ln (*k*/*T*) vs. the reciprocal of temperature.

$$\ln\frac{k}{T} = -\frac{\Delta H^{\ddagger}}{R}\left(\frac{1}{T}\right) + \ln\frac{k_B}{h} + \frac{\Delta S^{\ddagger}}{R} \qquad \text{(Equation 3)}$$

k indicates the rate constant, R is the molar gas constant (8.314 J/K·mol), T is the temperature at which the compounds were measured, $\Delta H^{\ddagger}$ is the enthalpy of activation, k_B is the Boltzmann's constant (1.381×10^{-23} J/K), h is Planck's constant (6.626×10^{-34} J·s), and $\Delta S^{\ddagger}$ is the entropy of activation. The enthalpy of activation $\Delta H^{\ddagger}$ and the entropy of activation $\Delta S^{\ddagger}$ were determined from the slope and intercept of the linear fit, respectively.

The Gibbs free energy of activation $\Delta G^{\ddagger}$ was then obtained from Equation 4.

$$\Delta G^{\ddagger} = \Delta H^{\ddagger} - T \times \Delta S^{\ddagger} \qquad \text{(Equation 4)}$$

The thermal half-life $t_{1/2}$ of DAs **1**-**4** was determined by first extrapolating the rate constant k at T = 298 K from the Eyring plot (Equation 3). The rate constant k was then applied to the exponential fit of fractional conversion α as a function of time at α = 0.5 to give $t_{1/2}$ at T = 298 K.

d. UV-vis absorption spectroscopy in solutions

UV-vis absorption spectra for all compounds were recorded using a Cary 60 Bio UV-vis spectrophotometer, employing a UV Quartz cuvette with a 10 mm path length. DAs **1**-**4** were dissolved in toluene, allowing for the observation of their gradual conversion back to monomers. The concentrations of PBs **1**-**4** were approximately 3.6×10^{-5} M, 3.3×10^{-5} M, 3.7×10^{-5} M, 4.6×10^{-5} M, respectively; the concentrations of DAs **1**-**4** were approximately 1.8×10^{-5} M, 1.7×10^{-5} M, 1.9×10^{-5} M, 2.3×10^{-5} M, respectively.

e. Thermal reversion kinetics measurement in solutions by UV-vis spectroscopy

DAs **1**-**4** were dissolved in toluene, allowing for the observation of their gradual conversion back to monomers. The concentrations of DAs **1**-**4** were approximately 1.8×10^{-5} M, 1.7×10^{-5} M, 1.9×10^{-5} M, 2.3×10^{-5} M, respectively. The reversion of DAs **1**-**4** in toluene was monitored at three different isothermal temperatures in dark. The change in the absorption of DAs **1**-**4** as a function time was monitored at 300 nm, 300 nm, 306 nm, 303 nm, respectively, and their half-lives were obtained based on Eyring-Polanyi plots.

f. Cycling test

The cycling test of the solid sample (100 mg) of compound **1** was carried out by repeated overnight 300 nm irradiation in biphasic conditions and 15-minute heating at 110 °C. NMR analysis was performed after each cycle in C_6D_6. The dimer was purified by hexane washing, and the collected filtrate was recycled for subsequent experiments.

g. Computational methods

All structural optimization calculations were performed using Becke's three-parameter hybrid exchange functionals, the Lee-Yang-Paar correlation functional, and Grimme's D3 dispersion force correction method (B3LYP-D3)[1, 2] with the 6–31 + G** basis set implemented in the Gaussian16 Revision B.01[3] suite of programs with default thresholds and algorithms. The stationary points were optimized without any symmetry assumptions and were characterized by frequency analysis at the same level of theory (the number of imaginary frequencies, NIMAG, was 0). The transition state optimizations were performed by single numerical differentiation. The structural optimization in the cavity reaction field in the solvent was performed using SCRF method based on polarizable continuum model.

ΔH_{calc} (kJ/mol) was defined as the enthalpy difference between 1 mol of DA and the corresponding 2 mol of PB in vacuum. The nucleus-independent chemical shift (NICS) values were calculated at the HF/6-31G** level of theory.[4, 5] The optimized structures, including the dummy atoms for NICS calculations and the Cartesian coordinates, are shown in Figure S41 and Tables S2-S7.

2. UV-vis absorption spectroscopy in solution

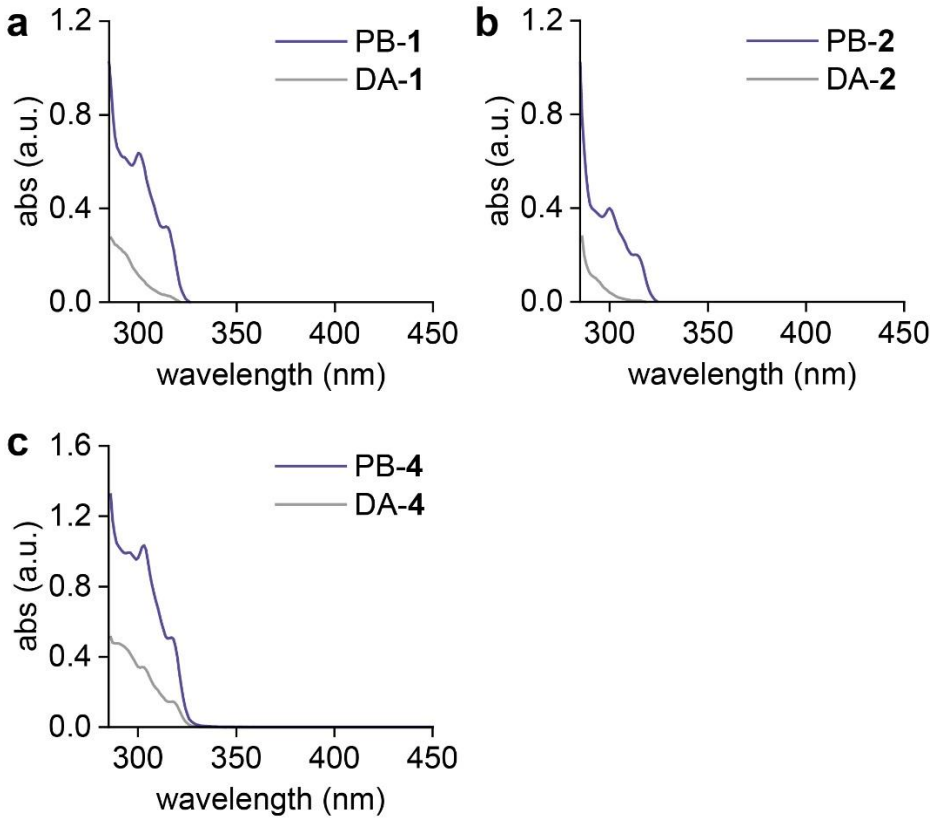

Figure S1. UV-vis absorption spectra of compounds (a) **1**, (b) **2** and (c) **4** in toluene. The concentrations of DA-**1**, DA-**2**, and DA-**4** were approximately 1.8×10^{-5} M, 1.7×10^{-5} M, and 2.3×10^{-5} M, respectively; and their reversion to monomers in solution was monitored until the full conversion was achieved.

3. Synthesis procedures of monomers and dimers

General synthesis of monomers

The reagent PB-**1**, obtained from Tokyo Chemical Industry Co., Ltd. (TCI), was further purified using silica gel column chromatography (0 to 10% ethyl acetate/hexanes) before being used in dimerization studies. PB-**2**, PB-**3**, and PB-**4** were synthesized and purified according to the reported procedures, and their identity was confirmed by comparing the obtained ^{1}H NMR spectra with the spectra published in the literature.[6-8]

General synthesis of dimers

To a 50 mL oven-dried, quartz round bottom flask, PB (100 mg) was added and dissolved in hexane (0.1 M for PBs **1**-**2**, 0.04 M for PB-**3**, and 0.01 M for PB-**4**). The solution was purged with N_2, followed by the addition of deaerated deionized water in 1:1 v/v ratio.[9] The biphasic mixture was irradiated without stirring in a Rayonet photoreactor chamber at 300 nm for 3-7 days. During irradiation, white precipitates formed at the interface of hexane/water. These precipitates were collected *via* vacuum filtration, then further purified by sonication in hexane (5 mL x 2), followed by the filtration with hexane rinsing.

To compare the dimerization yields between single-phase solution-state and biphasic conditions, the irradiation of PB-**1** (100 mg) was carried out in N_2-purged hexane. The results are summarized in Table S1.

Table S1. Conversion (%) of PB-**1** to DA-**1** in different reaction conditions.

entry	reaction medium	yield	reaction time
1	hexane	80%	4 days
2	hexane : water = 1:1	79%	3 days

4. NMR and FT-IR characterization of PBs and DAs

PB-1. ^{1}H NMR (400 MHz, C_6D_6) δ 8.29 (dd, J = 7.7, 2.1 Hz, 1H), 7.74 (dd, J = 7.7, 1.4 Hz, 1H), 7.13 – 6.94 (m, 3H). ^{13}C NMR (101 MHz, C6D6) δ 163.24, 151.32, 143.12, 131.38, 129.01, 127.93, 125.17, 124.76, 120.62, 110.70.

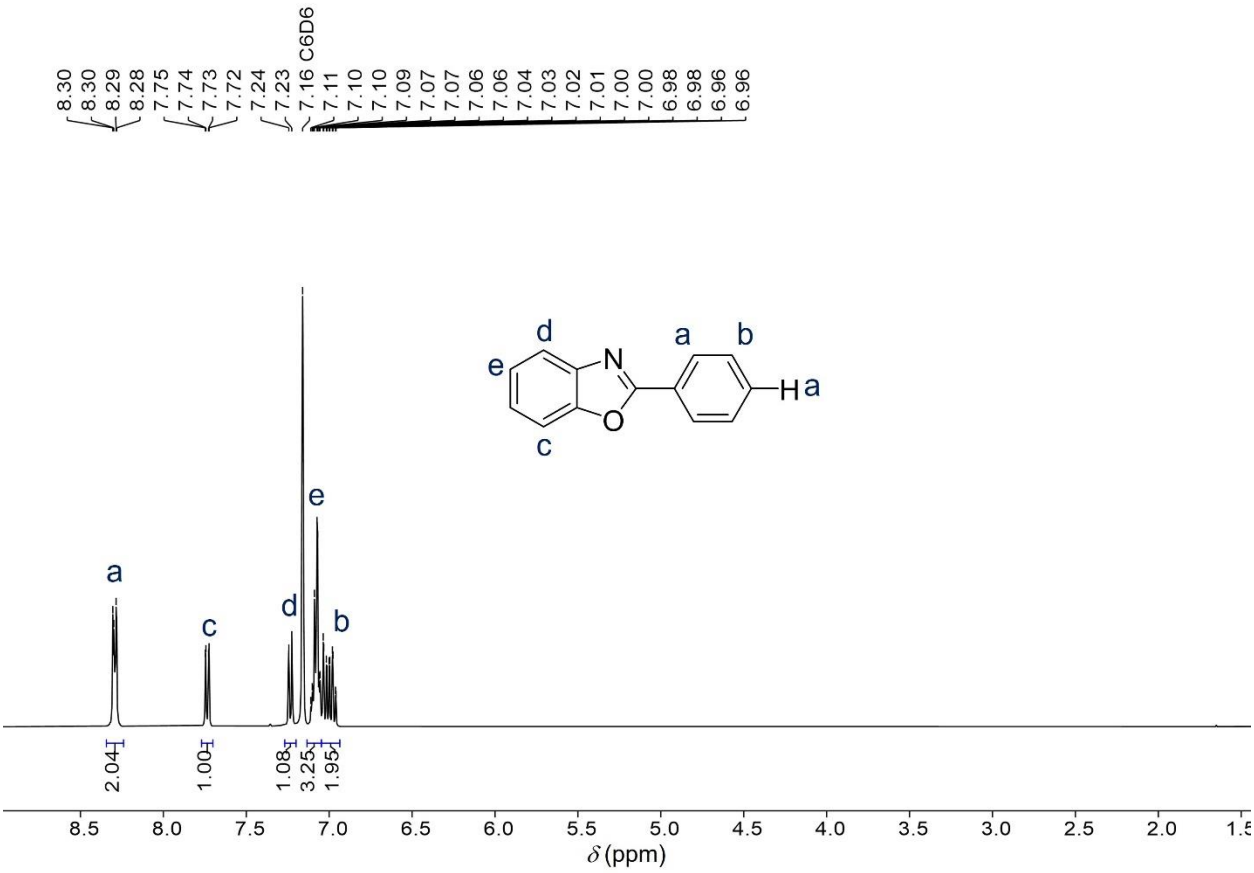

Figure S2. ^{1}H NMR spectrum of PB-**1**.

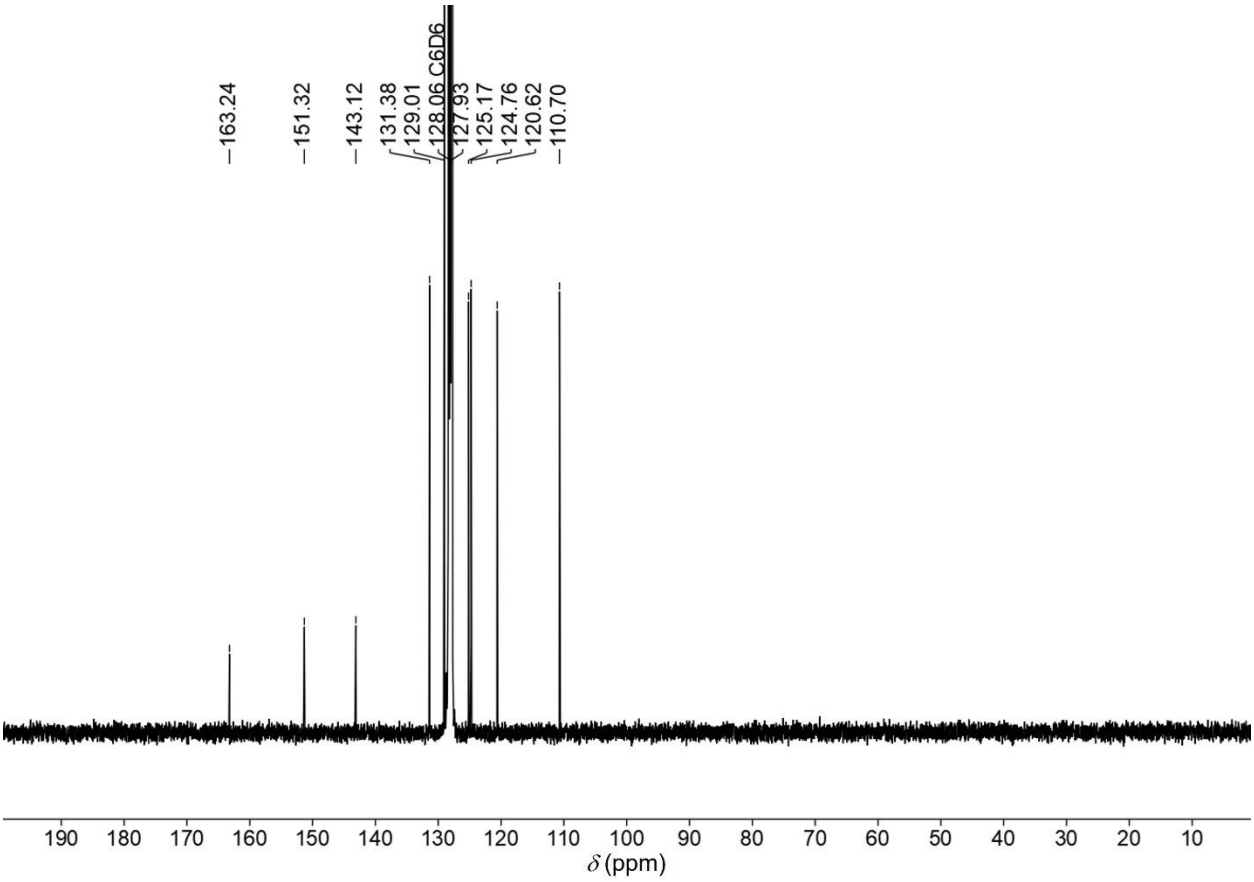

Figure S3. ^{13}C NMR spectrum of PB-**1**.

DA-1. 79% yield after 3 days of irradiation. ^{1}H NMR (400 MHz, C_6D_6) δ 8.28 (dt, J = 6.4, 2.5 Hz, 1H), 8.00 – 7.88 (m, 4H), 7.10 – 7.04 (m, 1H), 7.01 – 6.93 (m, 5H), 6.93 – 6.84 (m, 2H), 6.75 (dd, J = 7.9, 1.1 Hz, 2H), 6.56 (td, J = 7.8, 1.4 Hz, 2H), 6.48 (dd, J = 7.7, 1.3 Hz, 2H), 6.30 (td, J = 7.6, 1.1 Hz, 2H). ^{13}C NMR (101 MHz, C_6D_6) δ 155.00, 139.00, 135.24, 134.58, 131.40, 129.67, 129.02, 128.70, 127.01, 126.28, 125.16, 124.76, 122.87, 121.55, 120.62, 119.53, 110.69, 109.18.

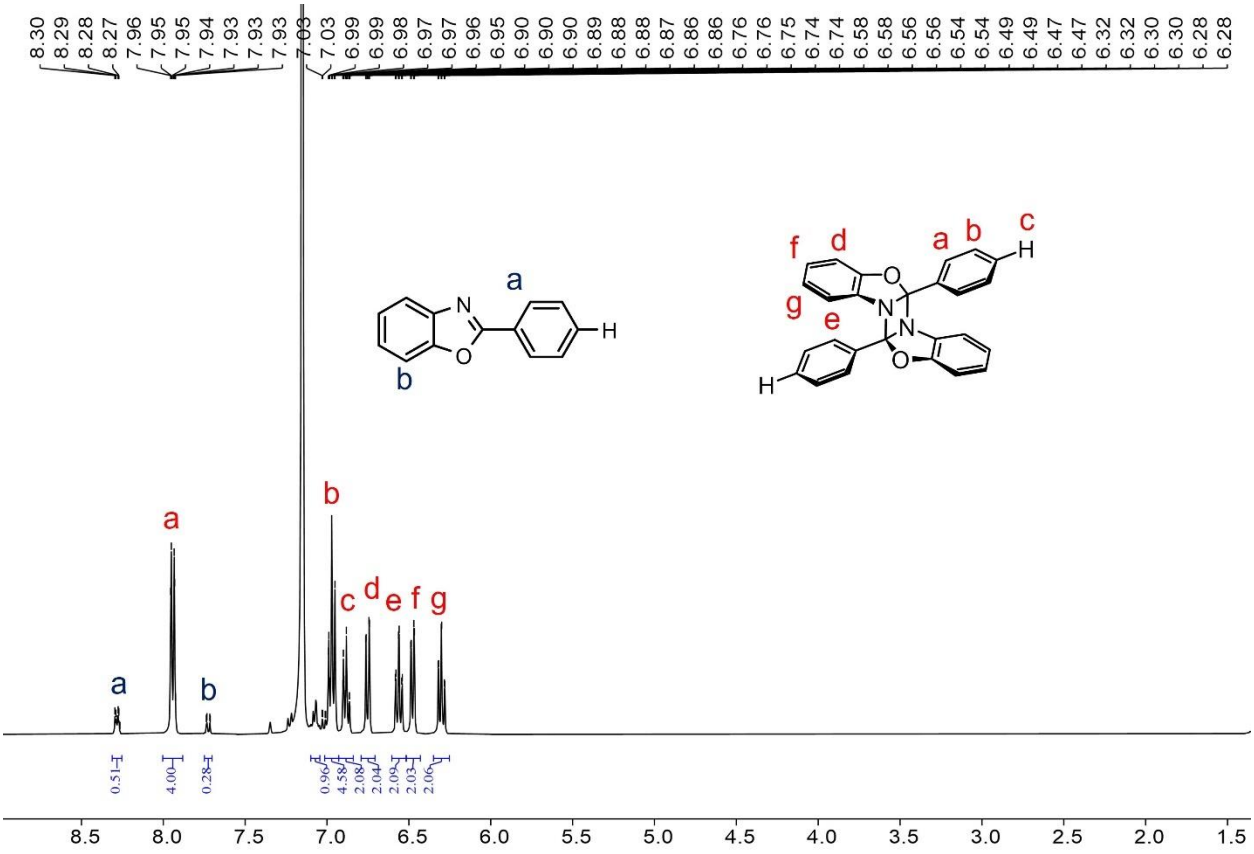

Figure S4. ^{1}H NMR spectrum of DA-**1**. The ratio of DA-**1** : PB-**1** was observed as 1 : 0.25 in C_6D_6 due to reversion in solution.

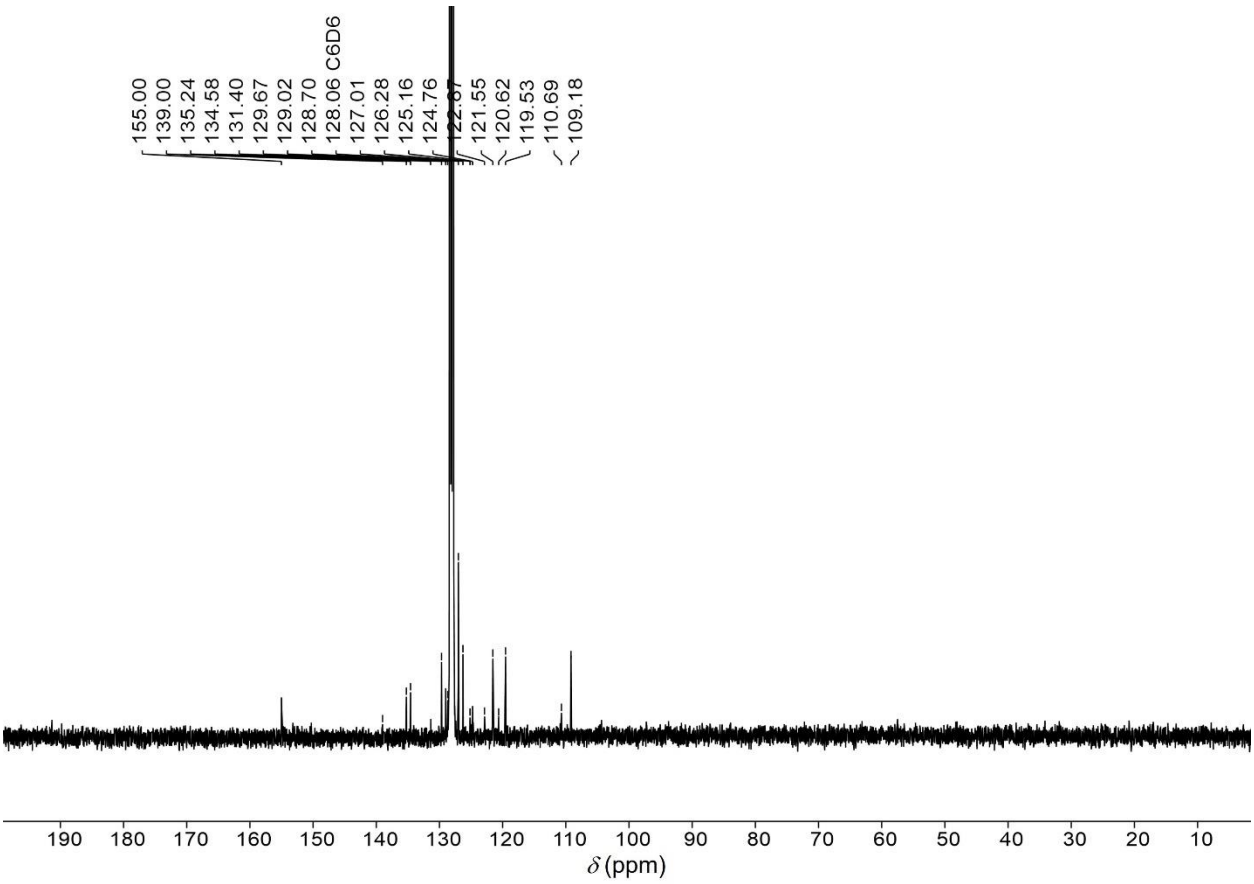

Figure S5. ^{13}C NMR spectrum of DA-**1**, containing PB-**1** due to reversion in solution.

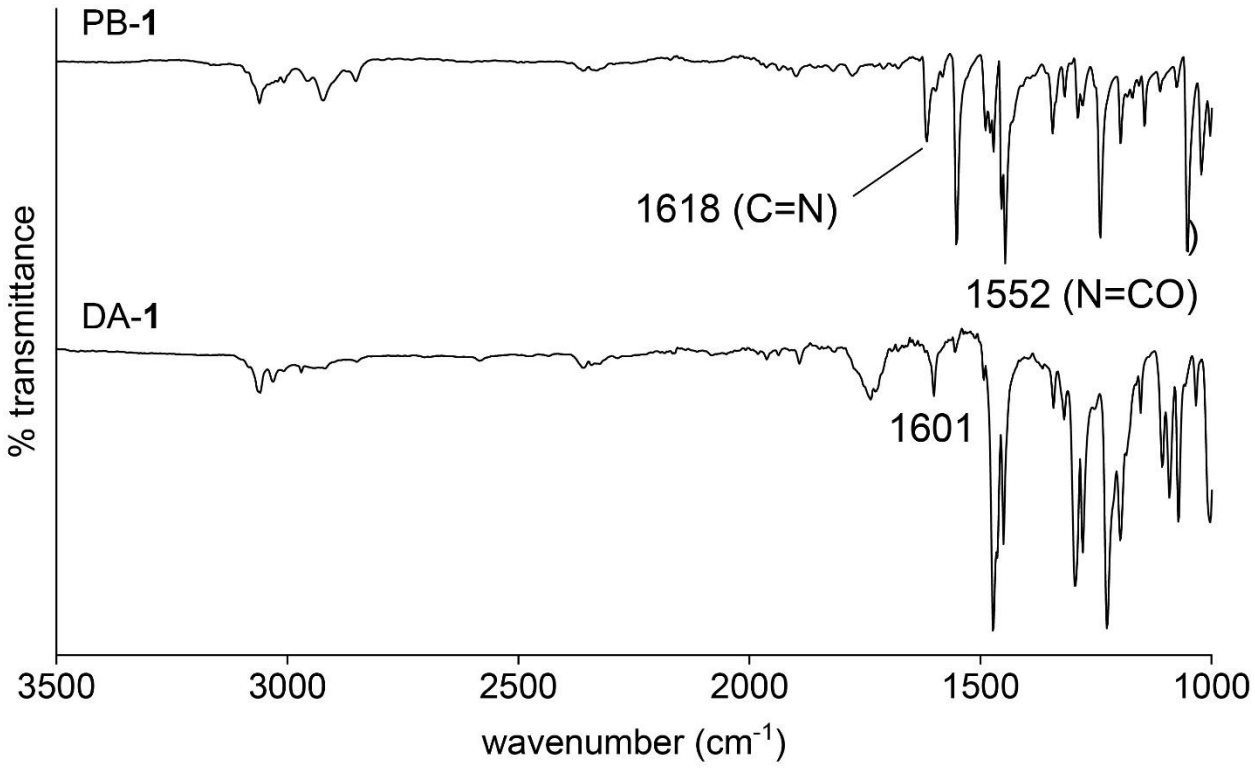

Figure S6. FT-IR spectra of PB-**1** and DA-**1**.

PB-2. ^{1}H NMR (400 MHz, C_6D_6) δ 8.02 (ddt, J = 9.2, 5.2, 1.1 Hz, 2H), 7.74 – 7.66 (m, 1H), 7.23 – 7.18 (m, 1H), 7.08 – 6.94 (m, 2H), 6.73 – 6.62 (m, 2H). ^{13}C NMR (101 MHz, C_6D_6) δ 166.23, 163.72, 162.30, 151.27, 143.01, 130.13, 130.04, 128.30, 128.06, 127.82, 125.19, 124.83, 124.10, 124.07, 120.56, 116.25, 116.03, 110.63. ^{19}F NMR (565 MHz, C_6D_6) δ -107.51.

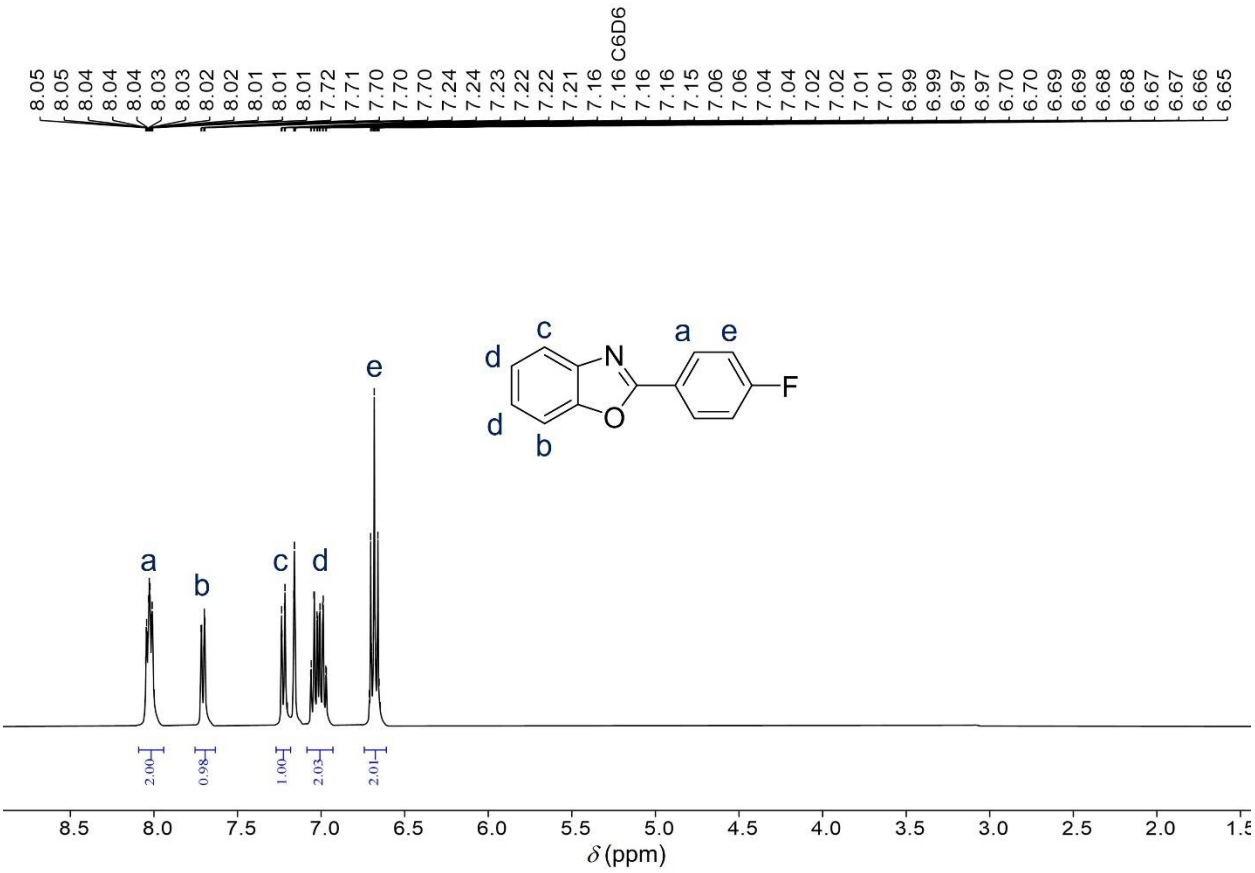

Figure S7. ^{1}H NMR spectrum of PB-**2**.

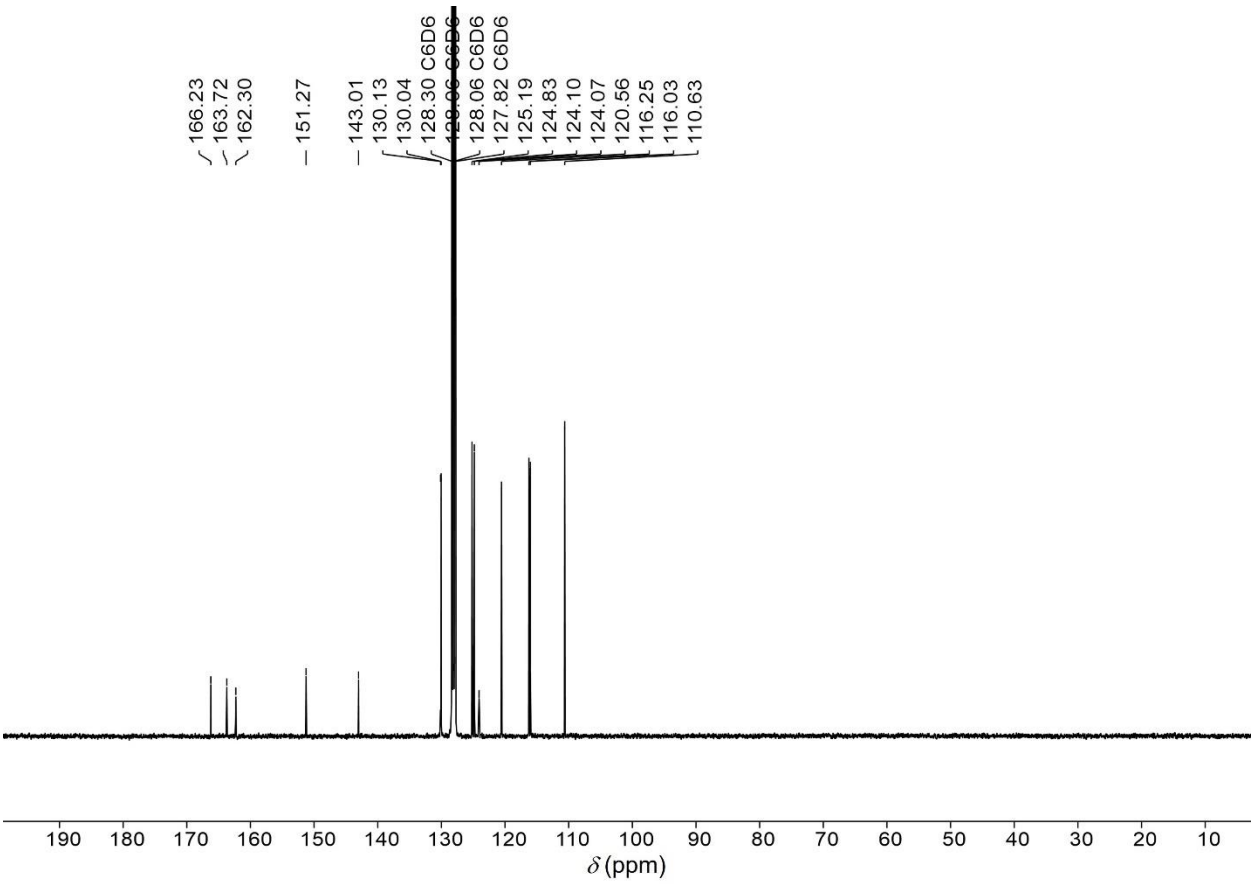

Figure S8. ^{13}C NMR spectrum of PB-**2**.

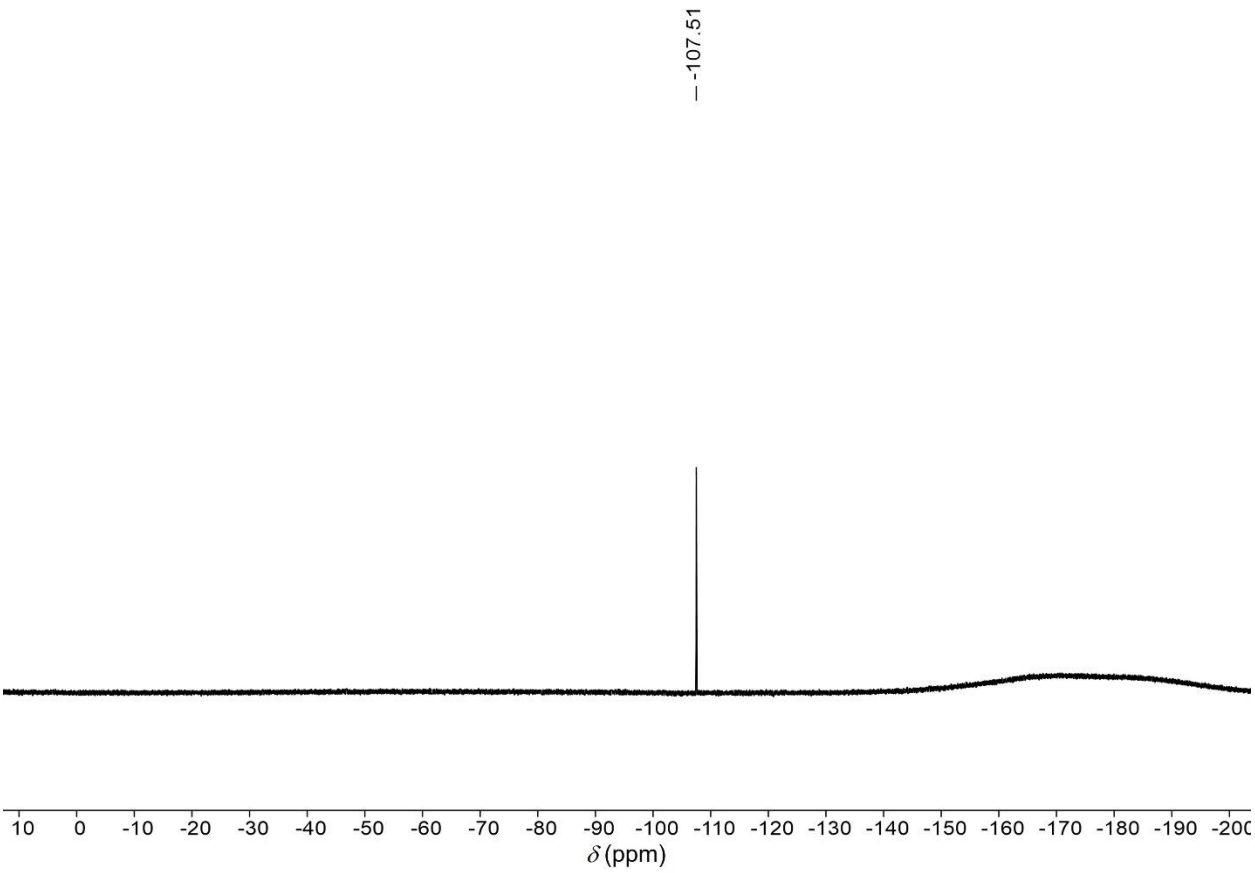

Figure S9. ^{19}F NMR spectrum of PB-**2**.

DA-2. 81% yield after 3.5 days of irradiation. ^{1}H NMR (400 MHz, C_6D_6) δ 7.83 – 7.73 (m, 2H), 6.80 (dd, J = 8.0, 1.1 Hz, 1H), 6.70 – 6.60 (m, 3H), 6.45 (dd, J = 7.7, 1.4 Hz, 1H), 6.37 (td, J = 7.6, 1.1 Hz, 1H). ^{13}C NMR (101 MHz, C_6D_6) δ 165.00, 162.52, 154.77, 134.25, 131.14, 130.15, 130.06, 129.15, 129.06, 128.70, 128.30, 128.18, 128.06, 127.94, 127.82, 126.56, 125.21, 124.85, 122.10, 121.82, 120.58, 119.41, 116.04, 115.36, 115.15, 110.64, 109.24. ^{19}F NMR (565 MHz, C_6D_6) δ -107.97, -111.08.

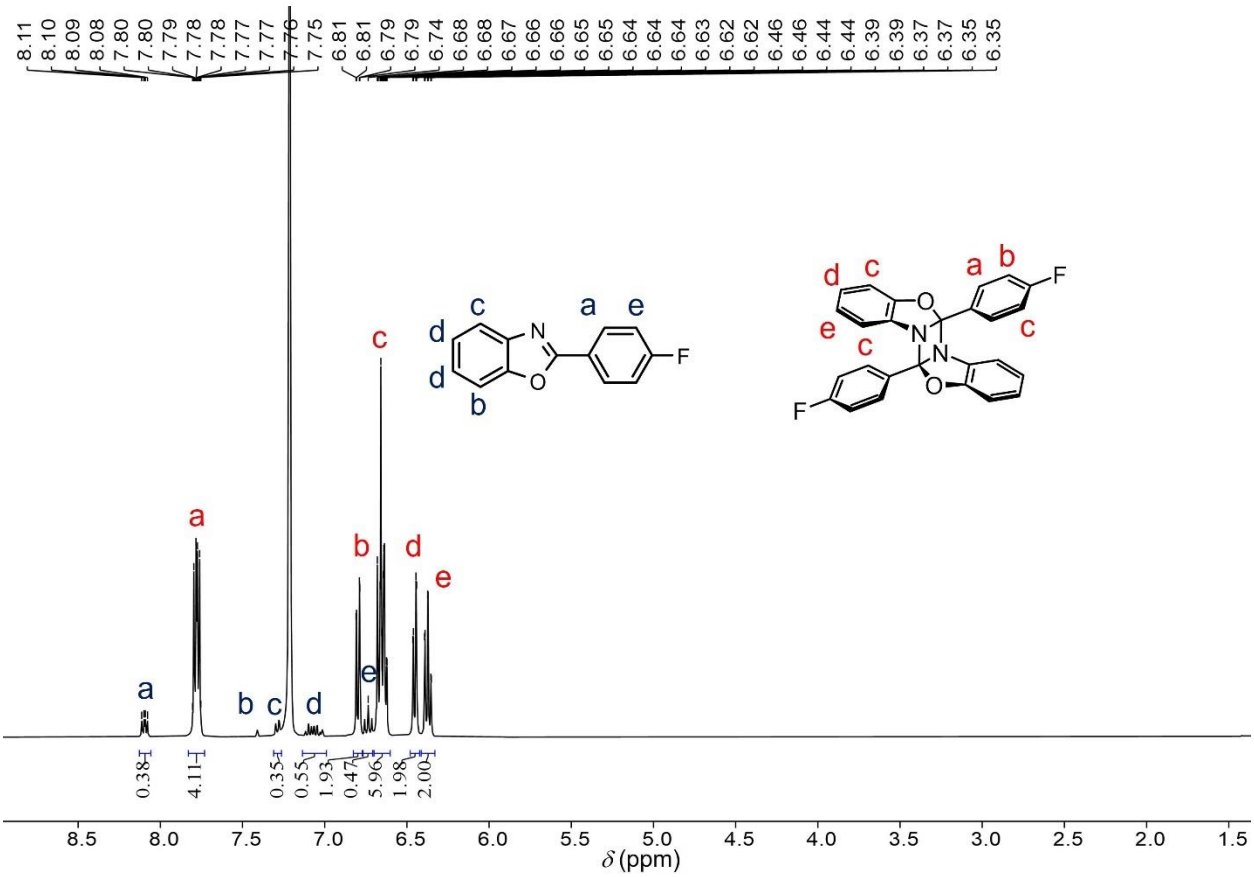

Figure S10. ^{1}H NMR spectrum of DA-**2**. The ratio of DA-**2** : PB-**2** was observed as 1 : 0.18 in C_6D_6 due to reversion in solution.

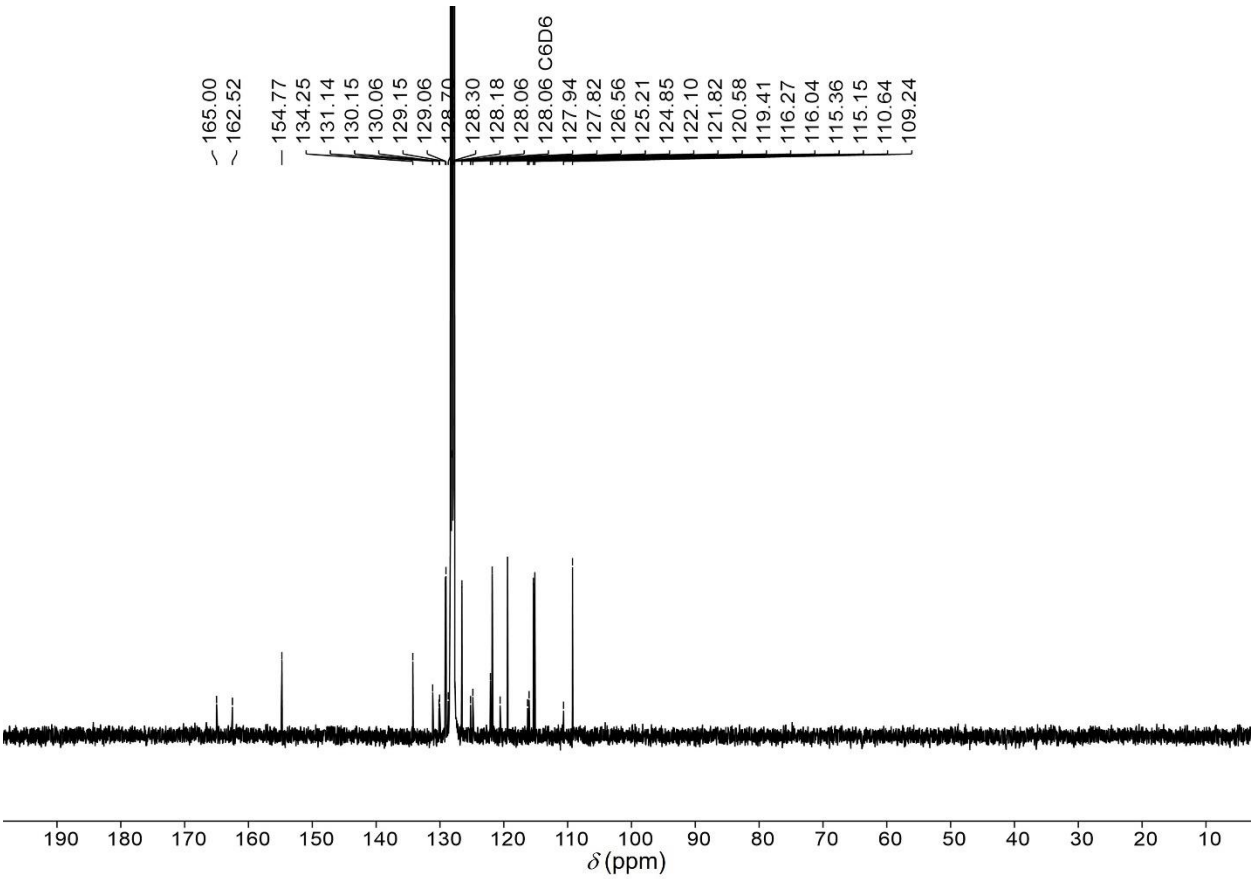

Figure S11. ^{13}C NMR spectrum of DA-**2**, containing PB-**2** due to reversion in solution.

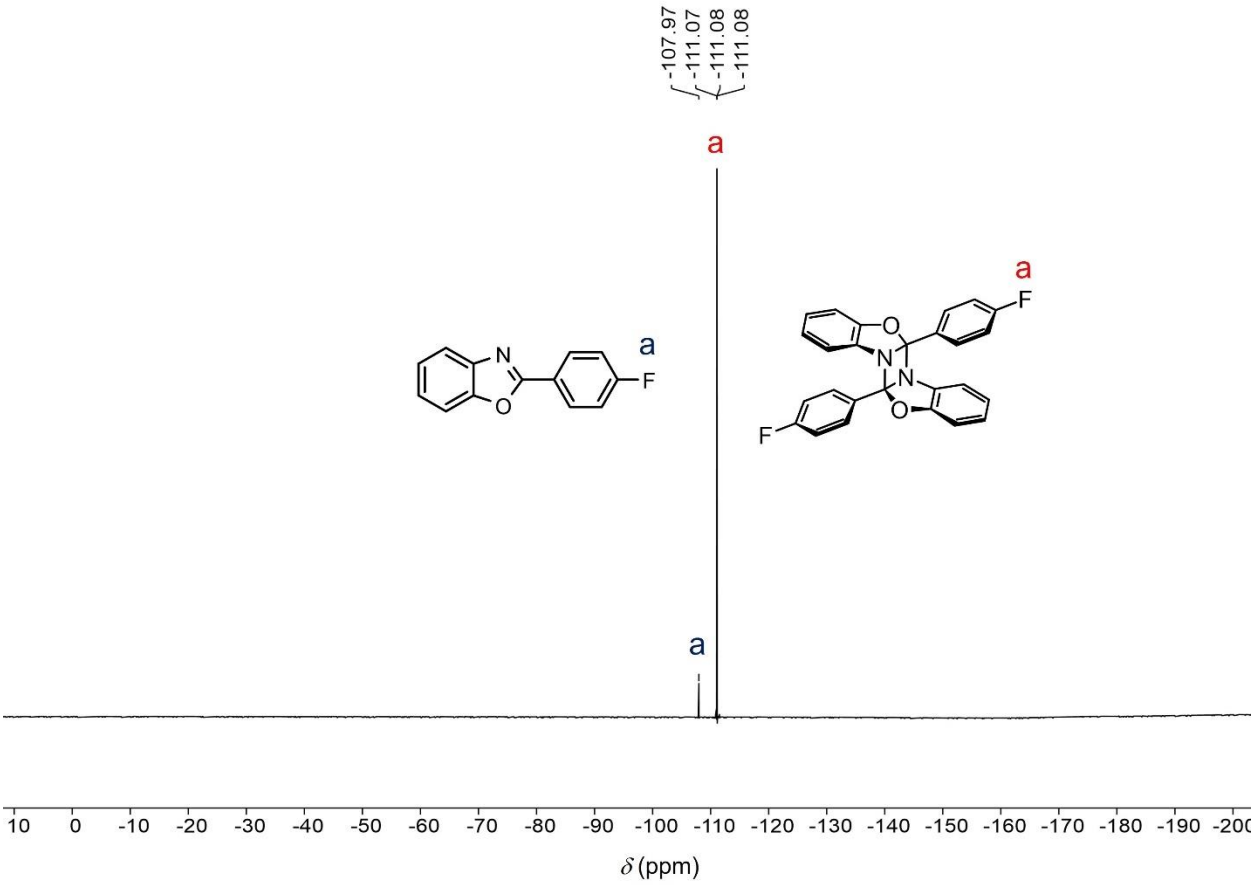

Figure S12. ^{19}F NMR spectrum of DA-**2**, containing PB-**2** due to reversion in solution.

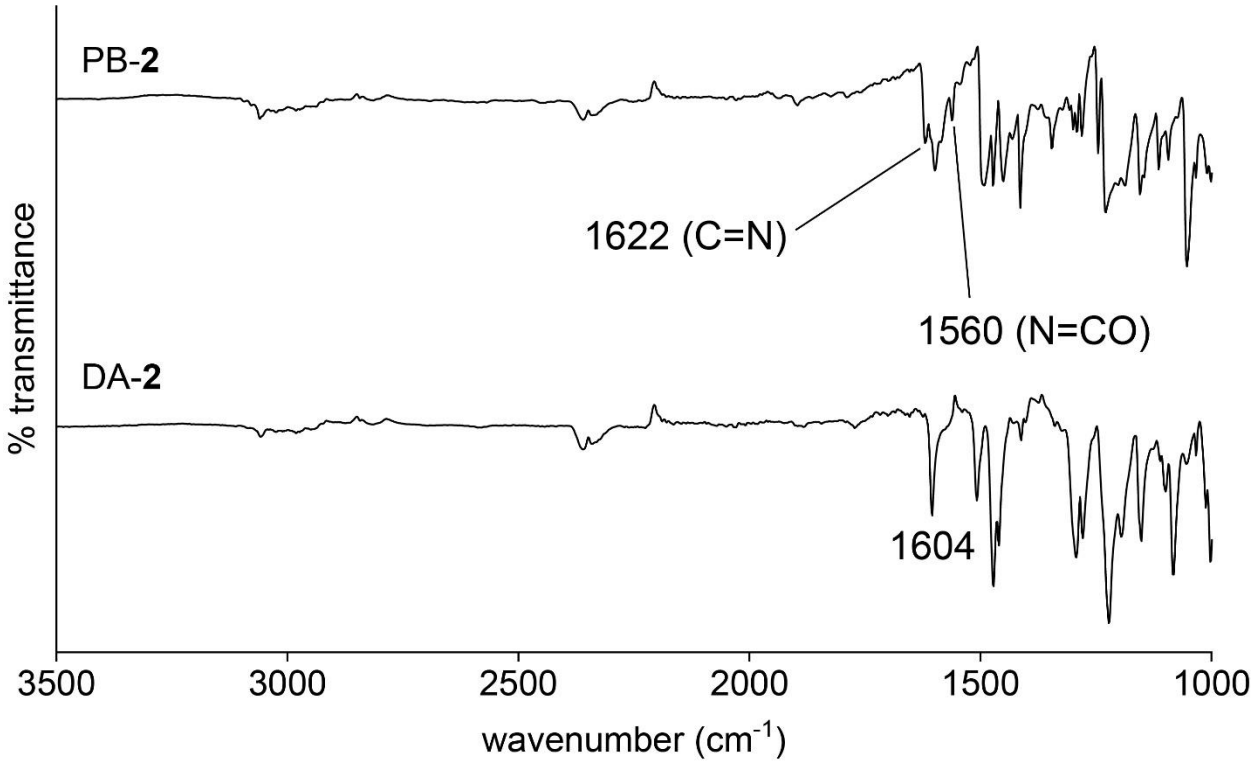

Figure S13. FT-IR spectra of PB-**2** and DA-**2**.

PB-3. ^{1}H NMR (400 MHz, C_6D_6) δ 7.96 (d, J = 8.8 Hz, 2H), 7.71 (dd, J = 8.0, 1.3 Hz, 1H), 7.25 – 7.19 (m, 1H), 7.08 – 6.94 (m, 3H). ^{13}C NMR (101 MHz, C_6D_6) δ 162.22, 151.24, 142.95, 137.65, 129.35, 129.12, 126.23, 125.40, 124.92, 120.65, 110.69.

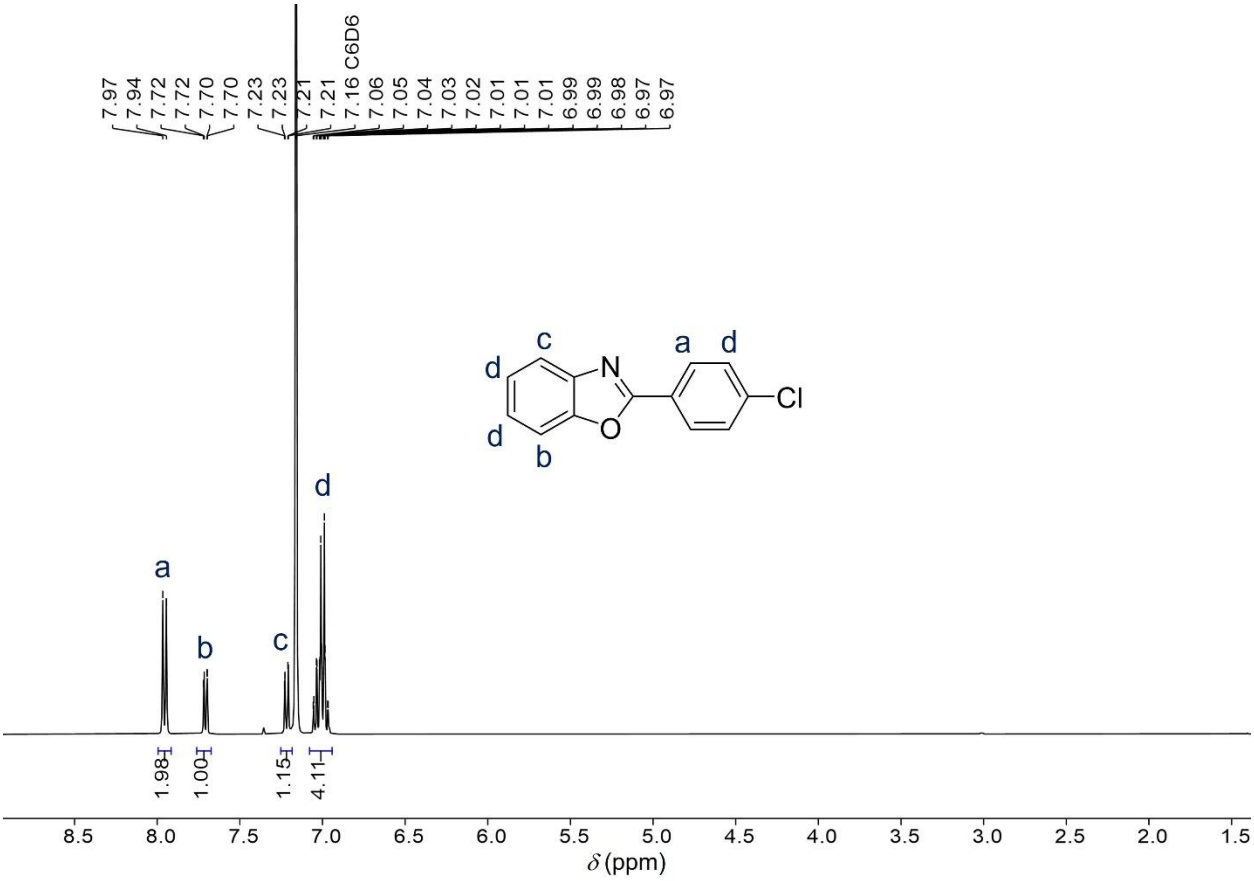

Figure S14. ^{1}H NMR spectrum of PB-**3**.

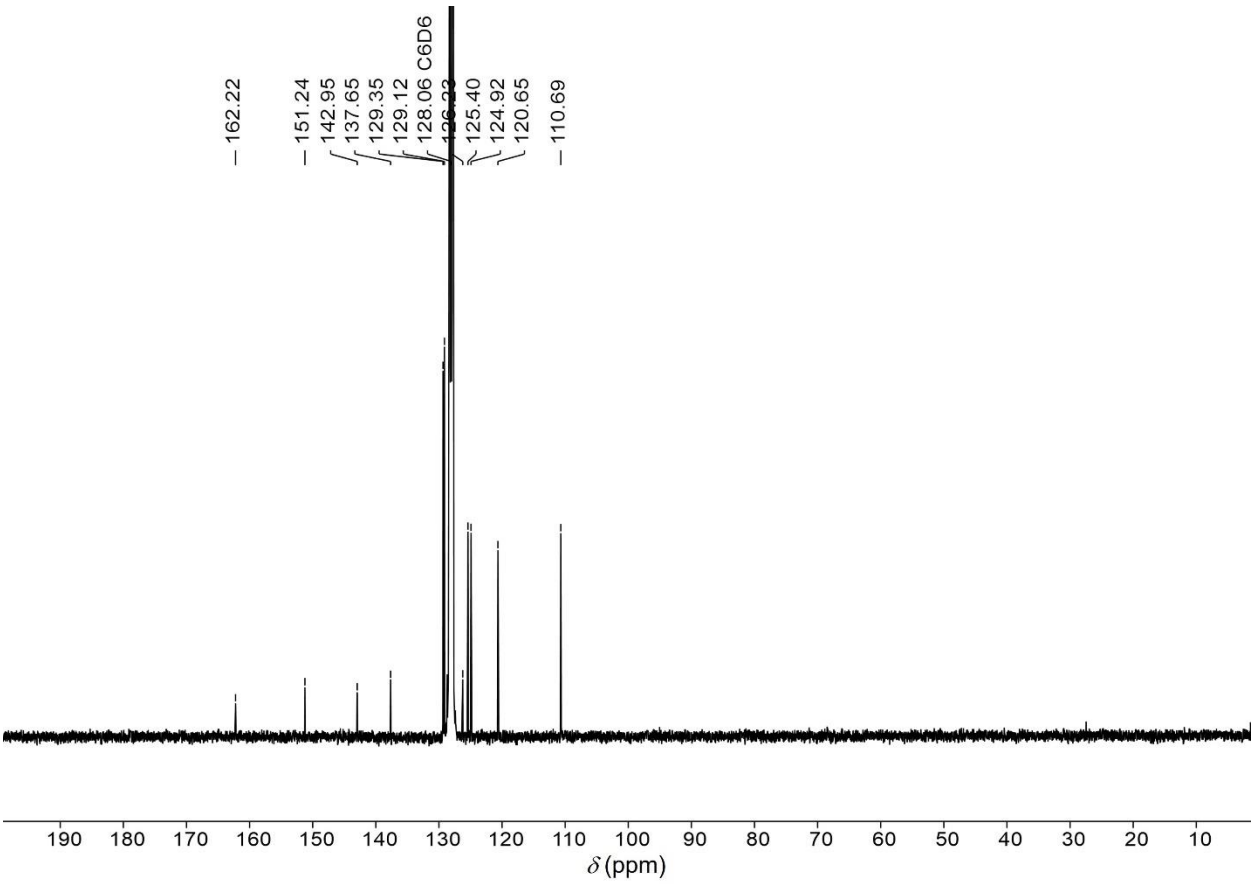

Figure S15. ^{13}C NMR spectrum of PB-**3**.

DA-3. 90% yield after 7 days of irradiation. ^{1}H NMR (400 MHz, C_6D_6) δ 7.68 – 7.60 (m, 2H), 6.91 (s, 2H), 6.72 (dd, J = 8.0, 1.1 Hz, 1H), 6.56 (td, J = 7.8, 1.4 Hz, 1H), 6.38 (dd, J = 7.7, 1.4 Hz, 1H), 6.28 (td, J = 7.6, 1.1 Hz, 1H). ^{13}C NMR (101 MHz, C_6D_6) δ 154.67, 136.02, 134.04, 133.52, 129.35, 129.13, 128.56, 128.43, 128.30, 128.06, 127.82, 126.68, 125.40, 124.92, 122.03, 121.93, 120.66, 119.39, 110.69, 109.26.

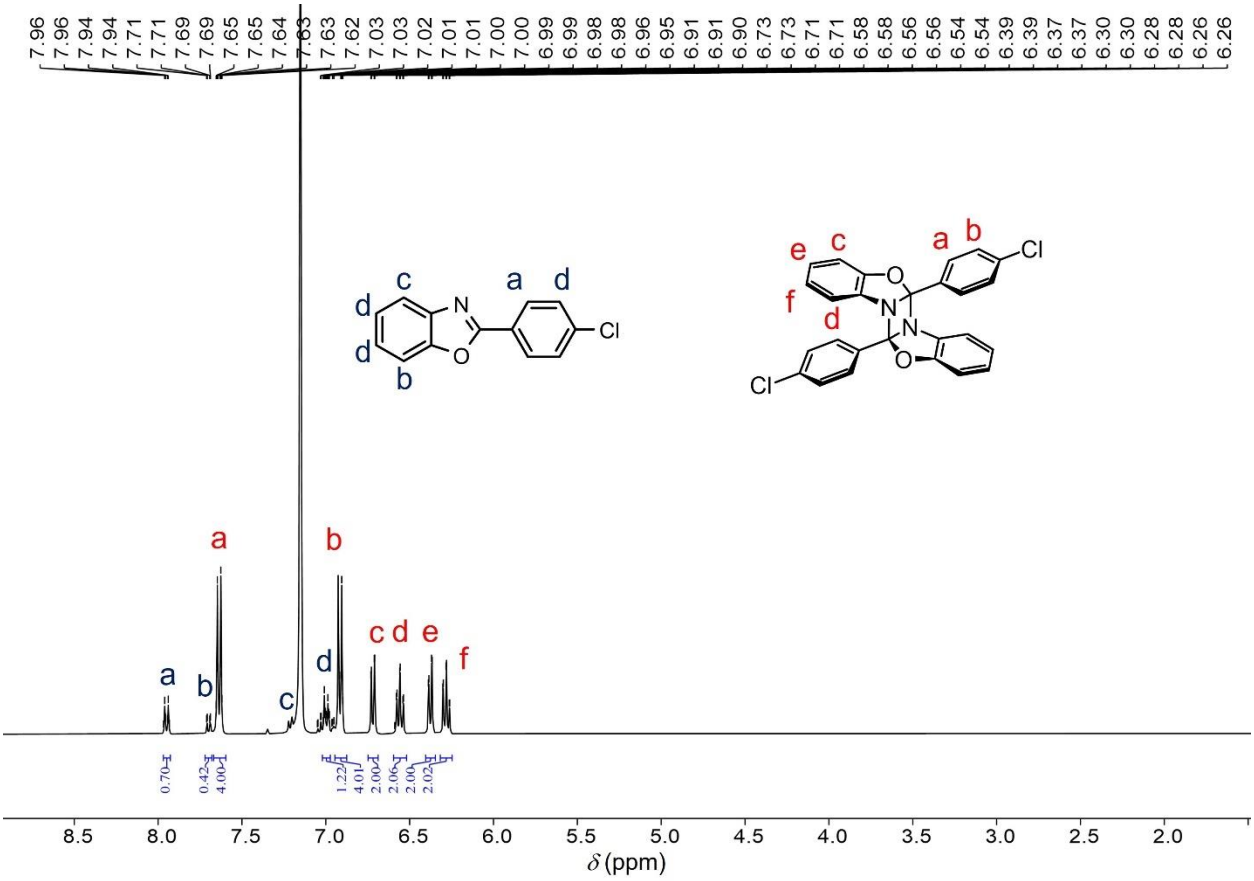

Figure S16. ^{1}H NMR spectrum of DA-**3**. The ratio of DA-**3** : PB-**3** was observed as 1 : 0.35 in C_6D_6 due to reversion in solution.

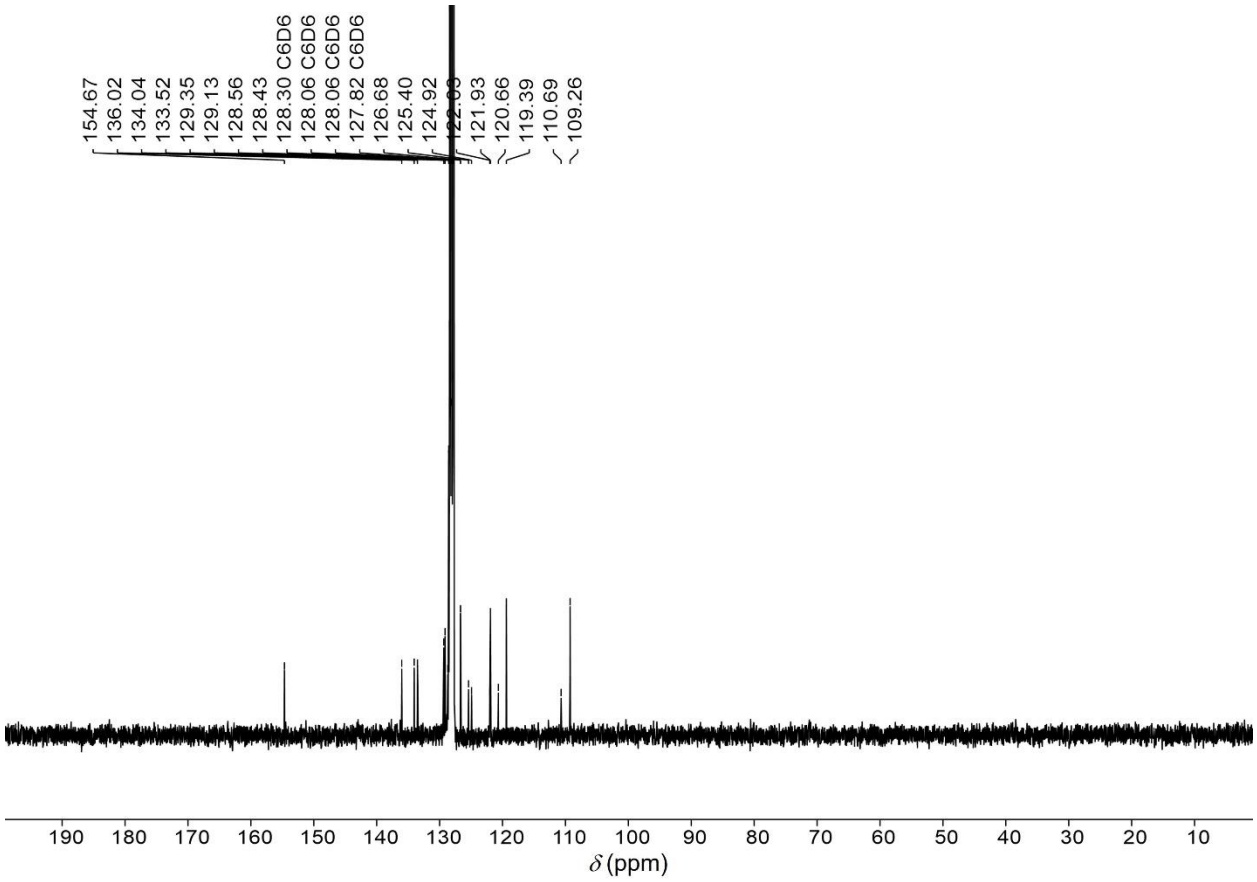

Figure S17. ^{13}C NMR spectrum of DA-**3**, containing PB-**3** due to reversion in solution.

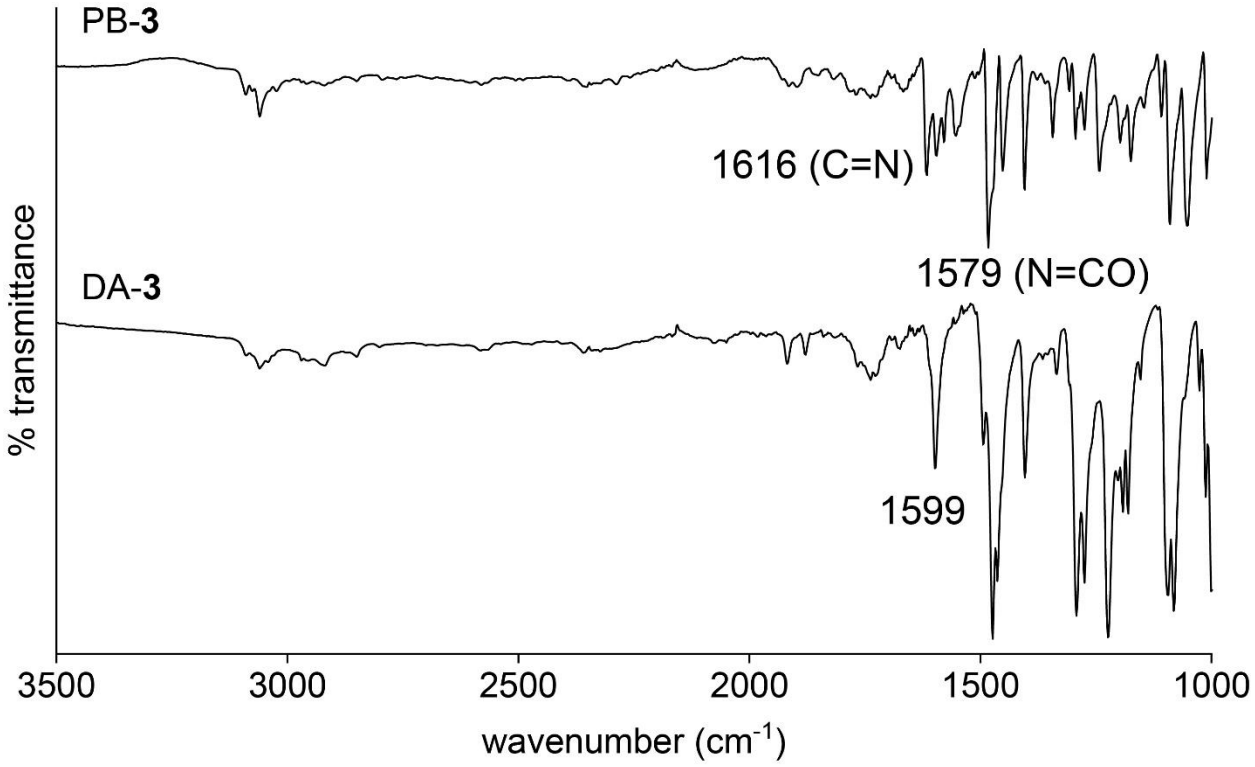

Figure S18. FT-IR spectra of PB-**3** and DA-**3**.

PB-4. ^{1}H NMR (400 MHz, C_6D_6) δ 8.30 – 8.21 (m, 2H), 7.75 (d, J = 7.7 Hz, 1H), 7.26 (d, J = 8.0 Hz, 1H), 7.02 (dt, J = 24.2, 7.6 Hz, 2H), 6.91 (d, J = 7.9 Hz, 2H), 1.99 (s, 3H). ^{13}C NMR (101 MHz, C_6D_6) δ 163.53, 151.29, 143.24, 141.79, 129.83, 129.01, 128.30, 128.06, 127.99, 127.82, 125.31, 124.97, 124.70, 120.48, 110.62, 21.37.

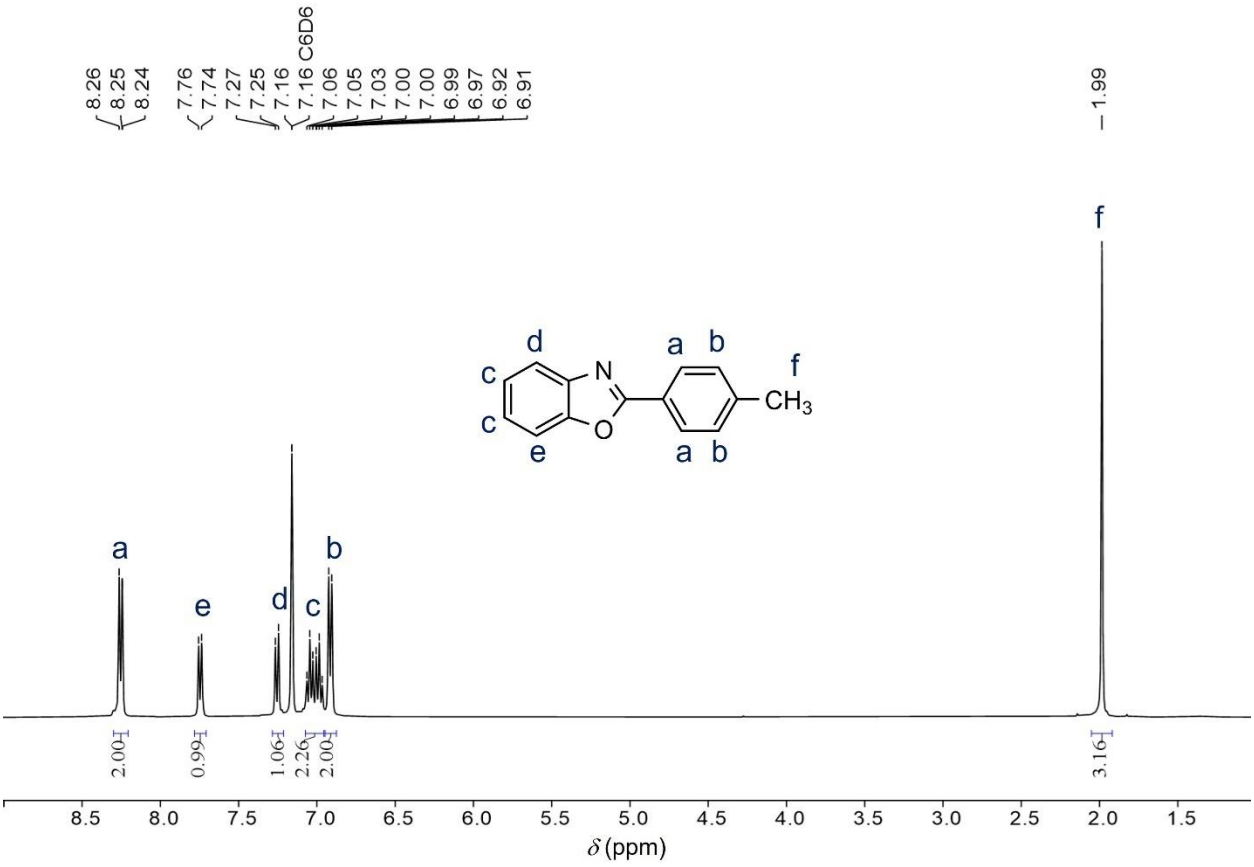

Figure S19. ^{1}H NMR spectrum of PB-**4**.

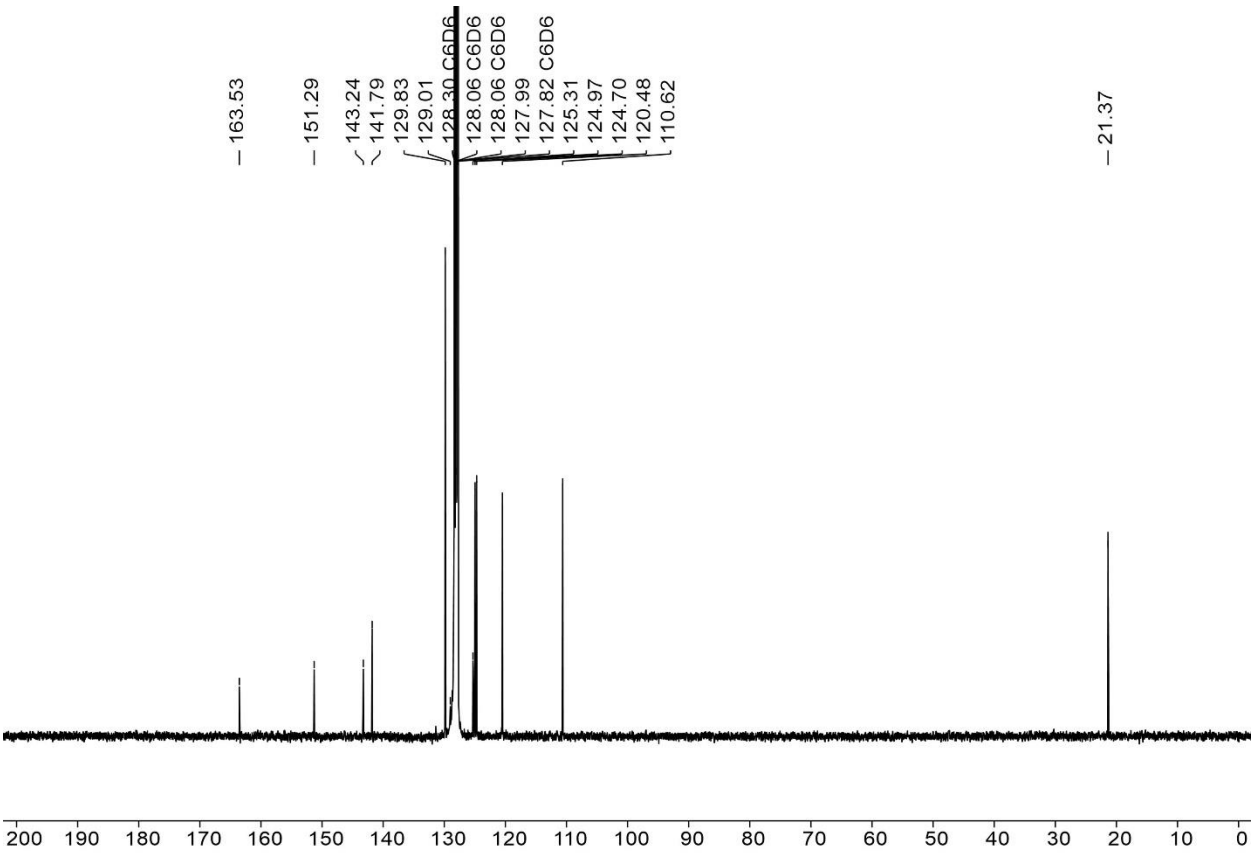

Figure S20. ^{13}C NMR spectrum of PB-**4**.

DA-**4**. 65% yield after 3 days of irradiation. ^{1}H NMR (400 MHz, C_6D_6) δ 7.95 – 7.87 (m, 4H), 6.81 (dd, J = 10.4, 7.8 Hz, 6H), 6.62 – 6.53 (m, 4H), 6.33 (td, J = 7.6, 1.1 Hz, 2H), 1.86 (s, 6H). ^{13}C NMR (101 MHz, C_6D_6) δ 141.79, 139.49, 134.80, 129.84, 128.99, 128.06, 127.82, 127.06, 126.24, 125.33, 124.96, 124.70, 121.53, 119.63, 110.62, 109.13, 21.37.

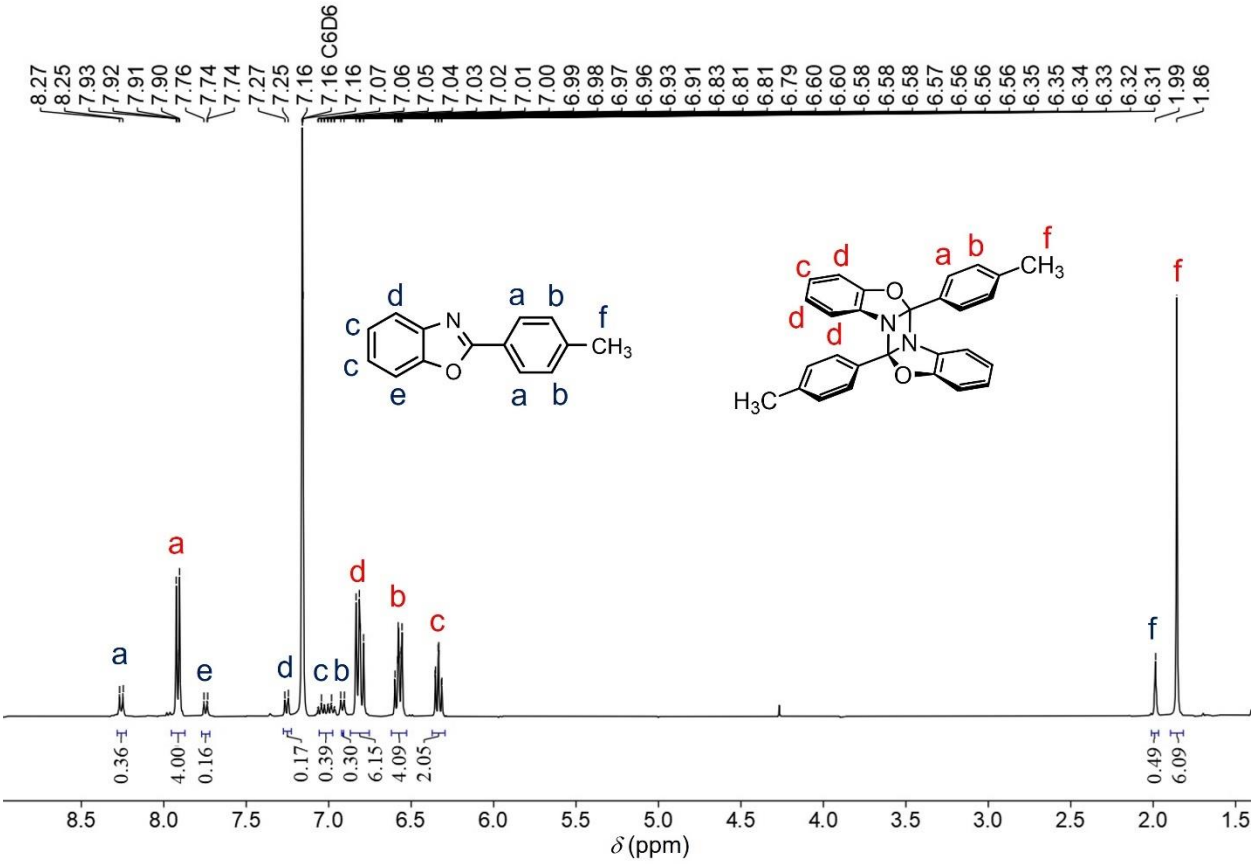

Figure S21. ^{1}H NMR spectrum of DA-**4**. The ratio of DA-**4** : PB-**4** was observed as 1 : 0.18 in C_6D_6 due to reversion in solution.

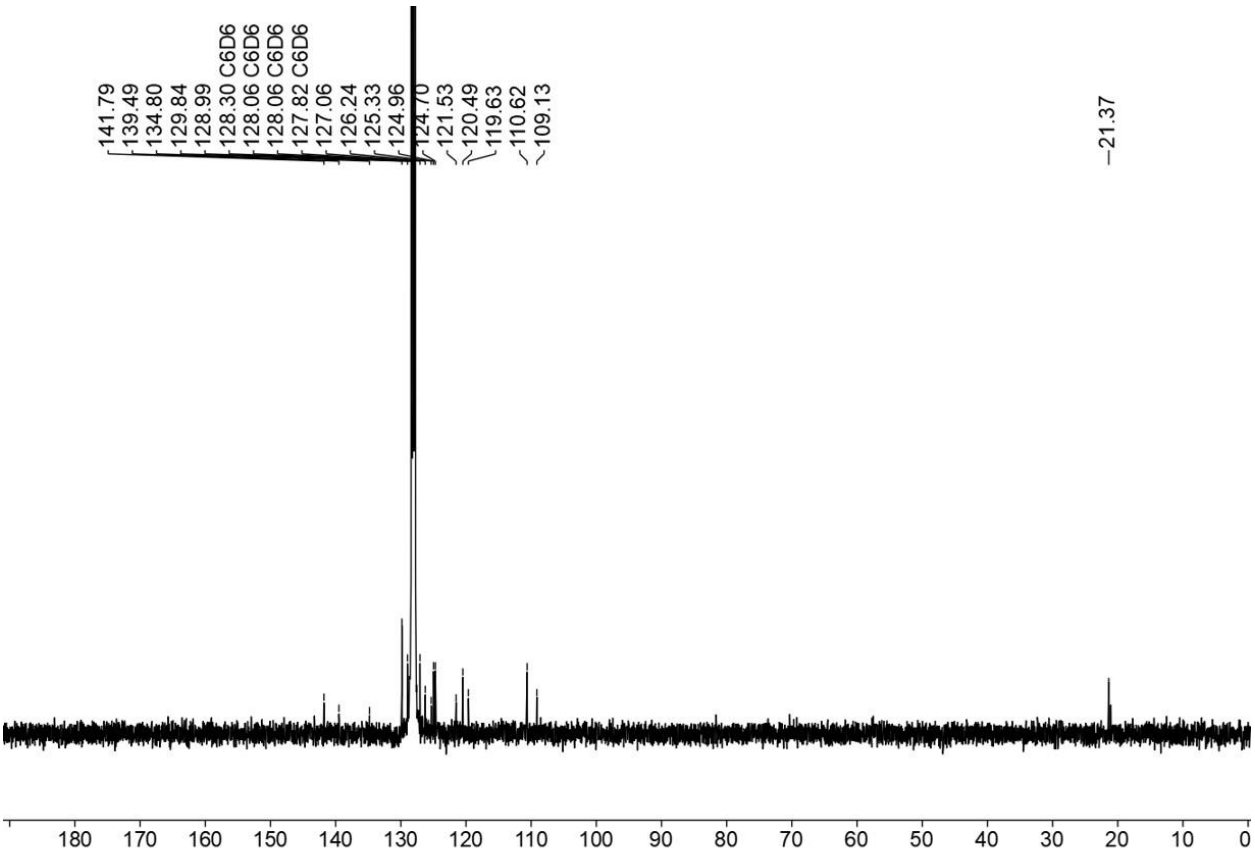

Figure S22. ^{13}C NMR spectrum of DA-**4**, containing PB-**4** due to reversion in solution.

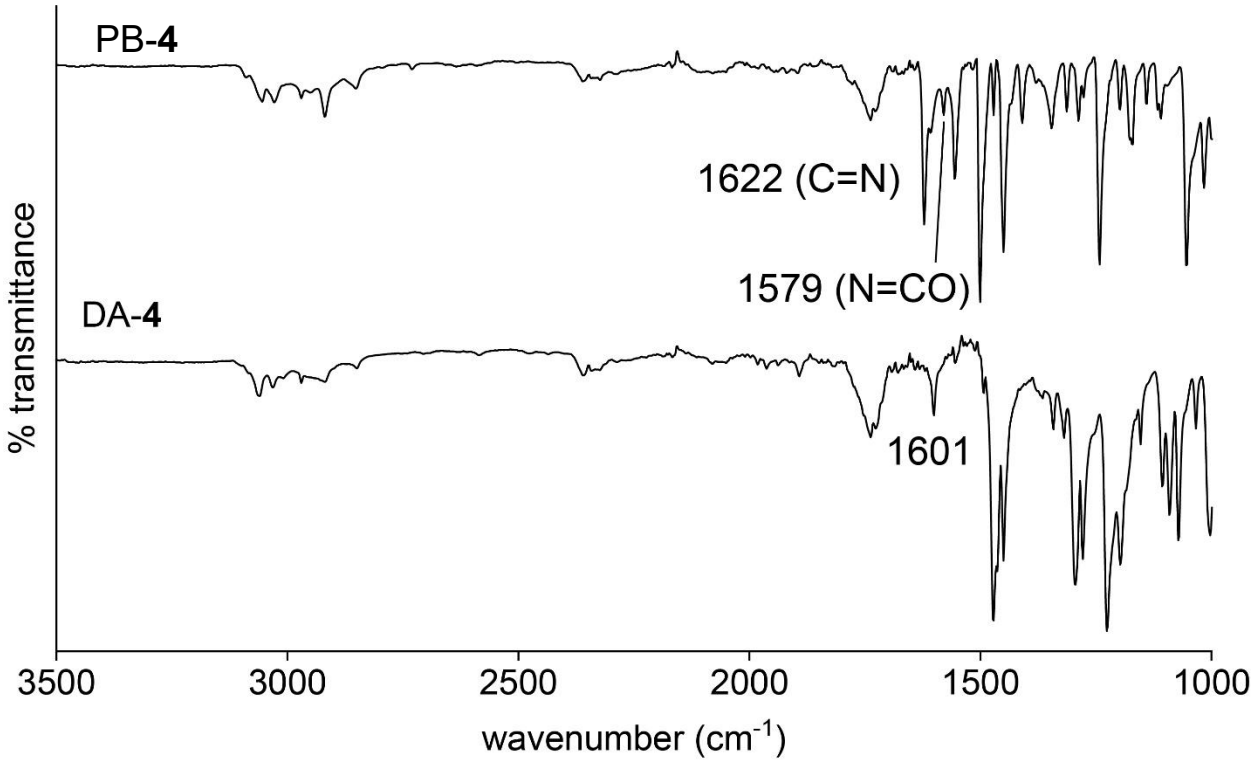

Figure S23. IR spectra of PB-**4** and DA-**4**.

5. Differential scanning calorimetry (DSC)

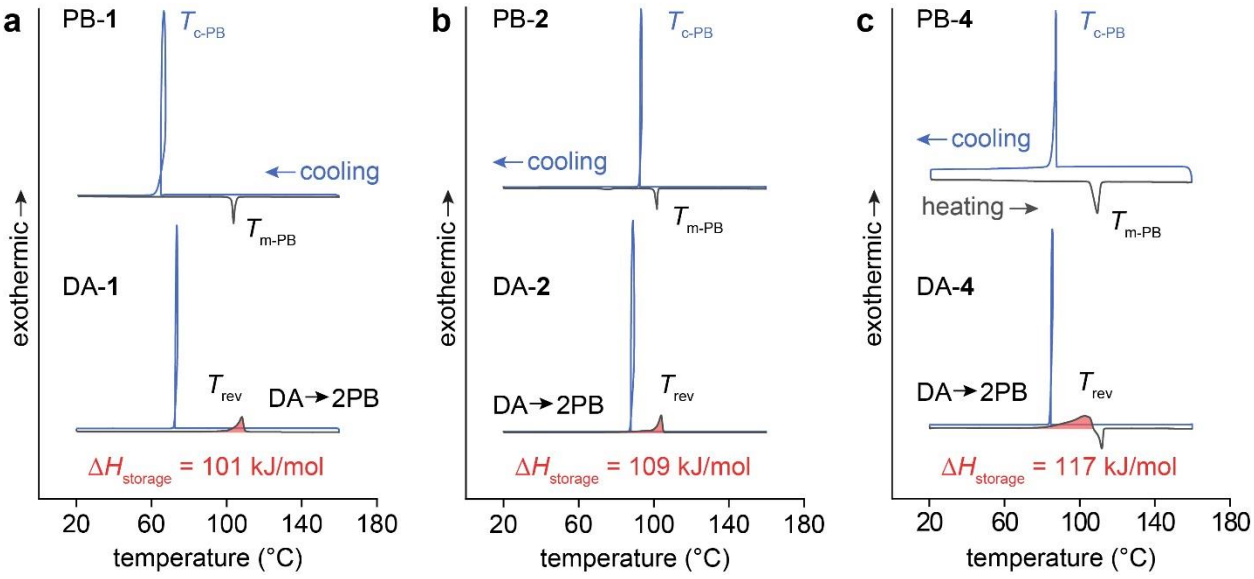

Figure S24. DSC plots of compounds (a) **1**, (b) **2** and (c) **4**. The melting points of PBs **1**, **2** and **4** are 101 °C, 102 °C, and 112 °C, respectively. The highlighted areas are integrated to obtain $\Delta H_{storage}$ values. T_{rev}: peak temperature of DA→2PB thermal reversion. $T_{m\text{-}PB}$: melting temperature of monomer. $T_{c\text{-}PB}$: crystallization temperature of monomer.

6. Cycling test

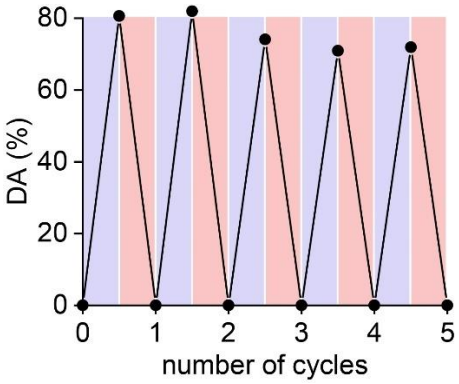

Figure S25. Cycling test of compound **1** upon repeated 300 nm irradiation and thermal activation.

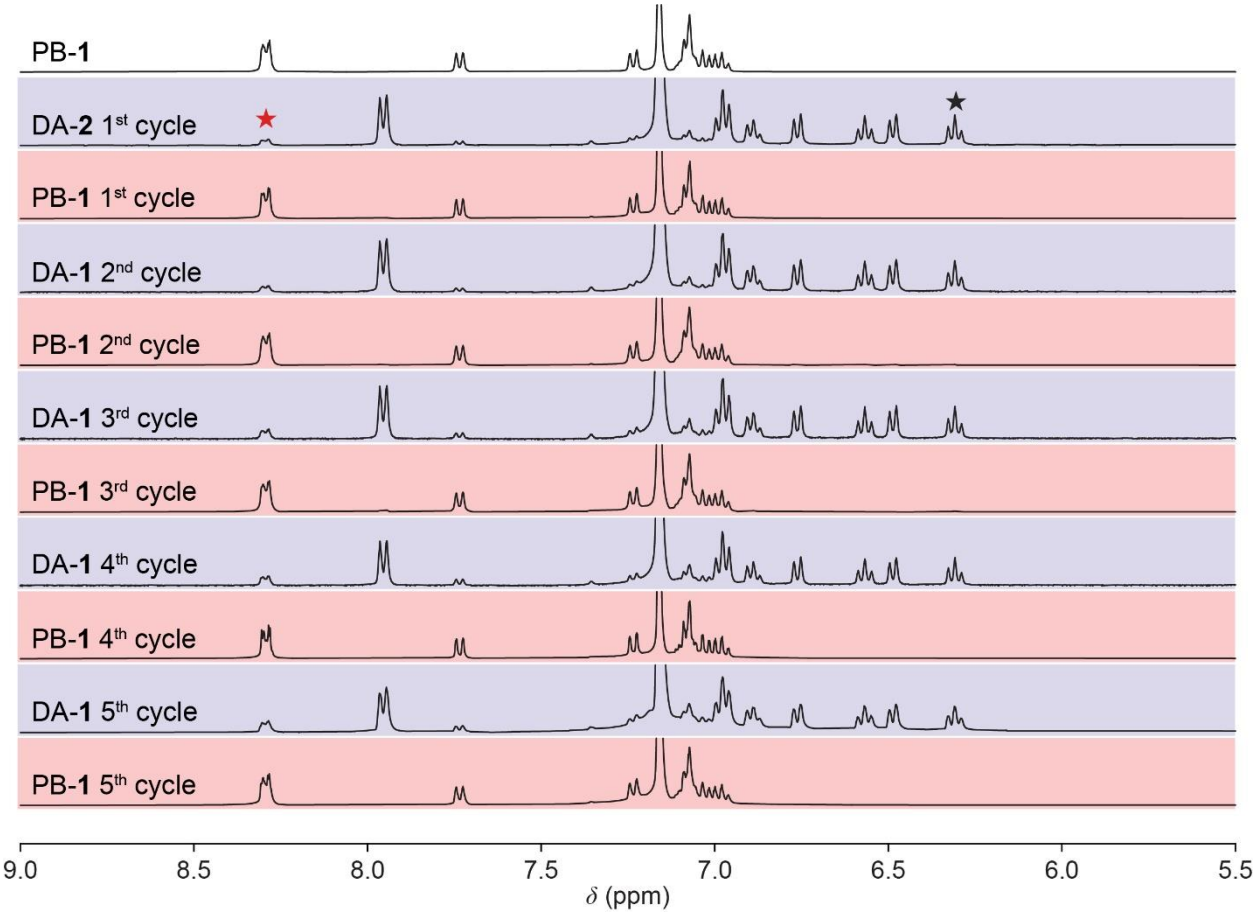

Figure S26. ^{1}H NMR spectra obtained from the cycling test of compound **1** upon repeated irradiation at 300 nm and heating at 110 °C in the solid sample showing no noticeable degradation. The %DA was quantified by comparing the peaks of the dimer (marked with a black star) and monomer (red star).

7. Isothermal DSC

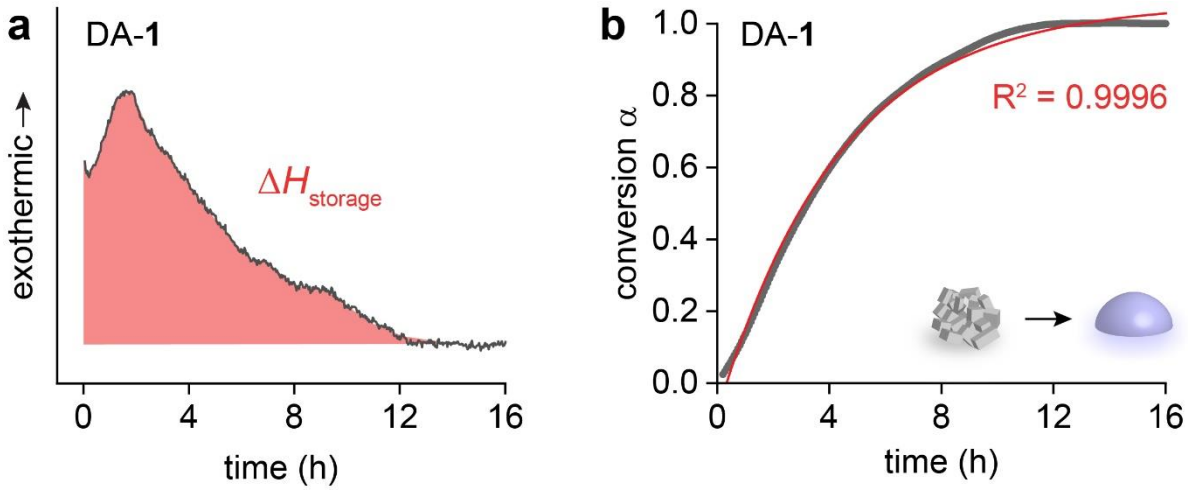

Figure S27. (a) A DSC thermogram of DA-**1** measured at 80 °C. (b) Conversion of DA-**1** over time at 80 °C. Red highlighted areas represent $\Delta H_{storage}$. The R^2 values are for the red curves fitted for 1st-order kinetics.

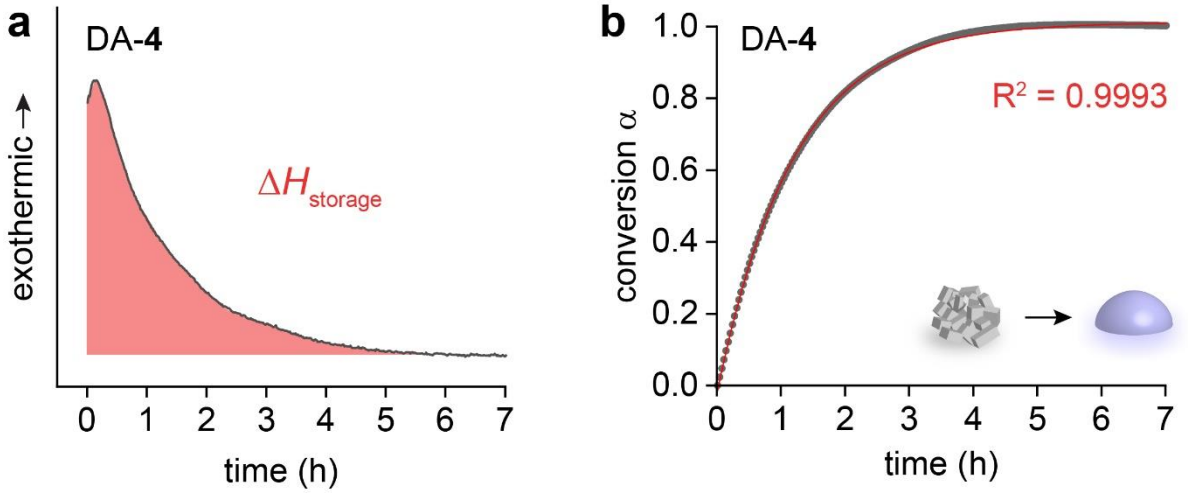

Figure S28. (a) A DSC thermogram of DA-**4** measured at 80 °C. (b) Conversion of DA-**4** over time at 80 °C. Red highlighted areas represent $\Delta H_{storage}$. The R^2 values are for the red curves fitted for 1st-order kinetics.

8. Thermal reversion kinetics measurement by DSC

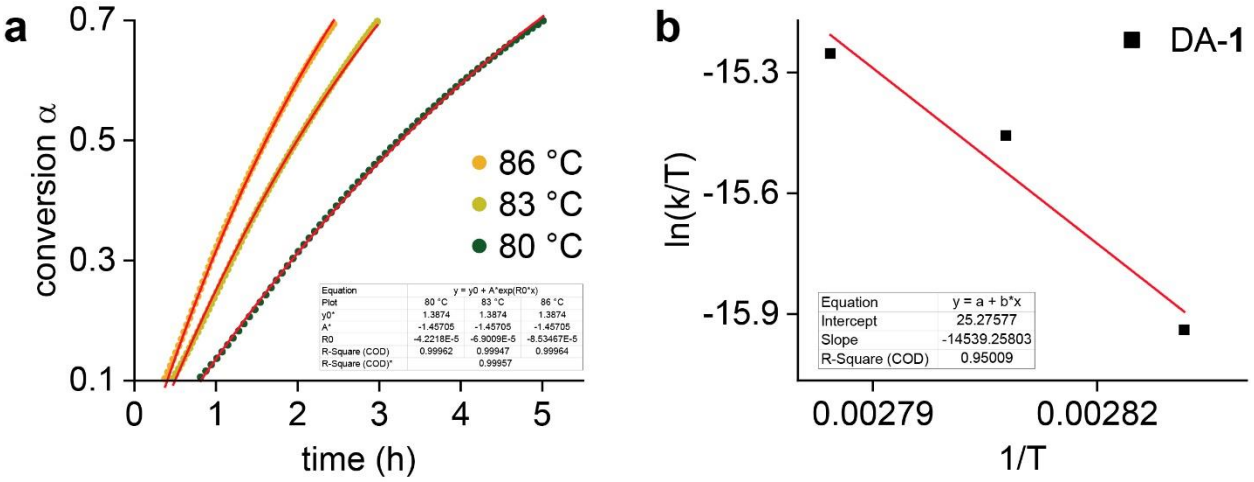

Figure S29. (a) The conversion of DA-**1** at 80 °C, 83 °C, and 86 °C, and the corresponding (b) Eyring plot. The conversion at each temperature was fitted to an exponential function. The fitted parameters were used to obtain the Eyring plot. The thermal half-life of DA-**1** at 25 °C was determined *via* the extrapolation of the Eyring plot.

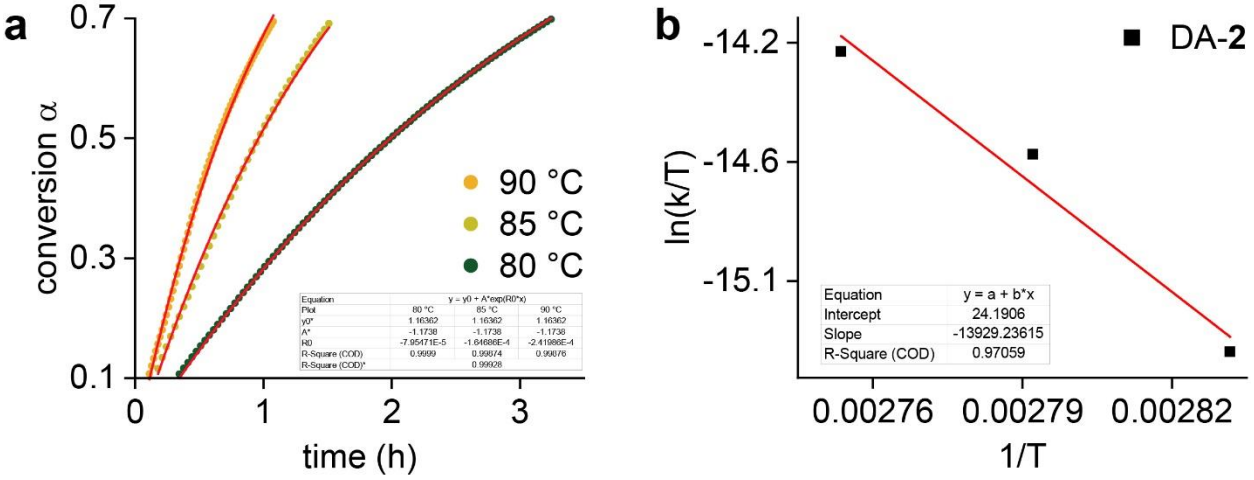

Figure S30. (a) The conversion of DA-**2** at 80 °C, 85 °C, and 90 °C, and the corresponding (b) Eyring plot. The conversion at each temperature was fitted to an exponential function. The fitted parameters were used to obtain the Eyring plot. The thermal half-life of DA-**2** at 25 °C was determined *via* the extrapolation of the Eyring plot.

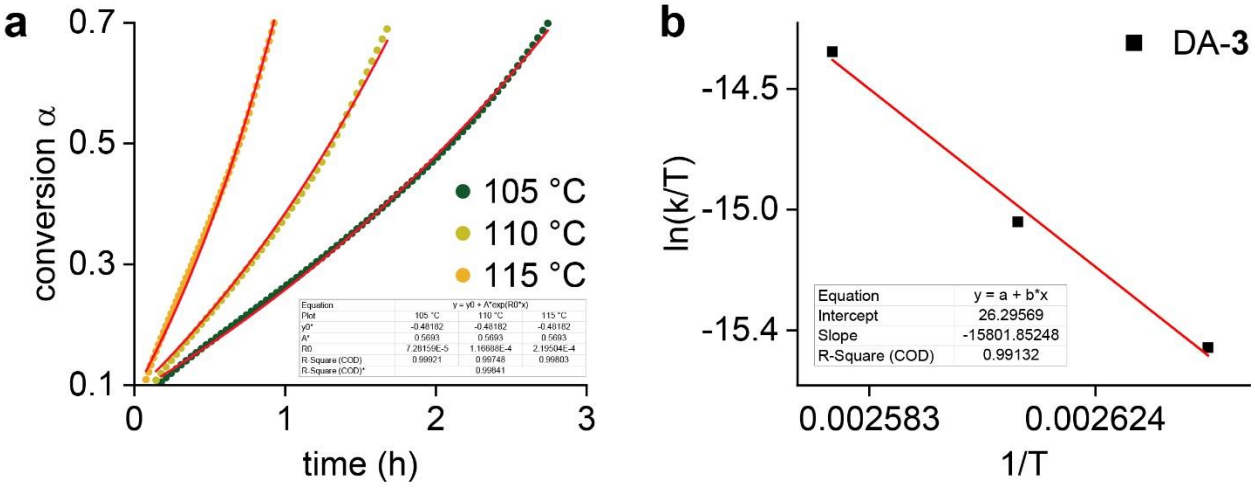

Figure S31. (a) The conversion of DA-**3** at 105 °C, 110 °C, and 115 °C, and the corresponding (b) Eyring plot. The conversion at each temperature was fitted to an exponential function. The fitted parameters were used to obtain the Eyring plot. The thermal half-life of DA-**3** at 25 °C was determined *via* the extrapolation of the Eyring plot.

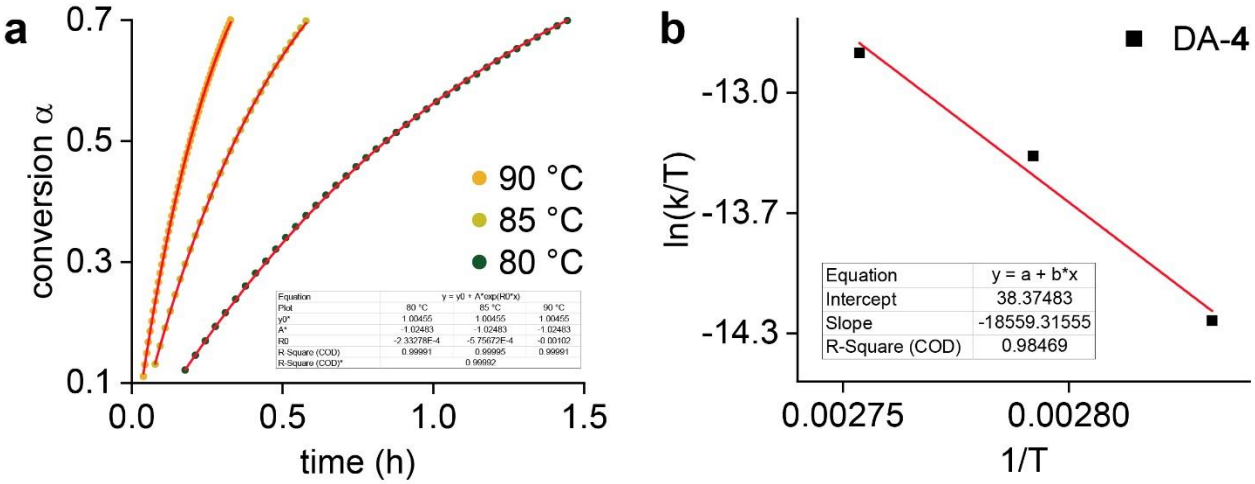

Figure S32. (a) The conversion of DA-**4** at 80 °C, 85 °C, and 90 °C, and the corresponding (b) Eyring plot. The conversion at each temperature was fitted to an exponential function. The fitted parameters were used to obtain the Eyring plot. The thermal half-life of DA-**4** at 25 °C was determined *via* the extrapolation of the Eyring plot.

9. Evaluation of solvation energy

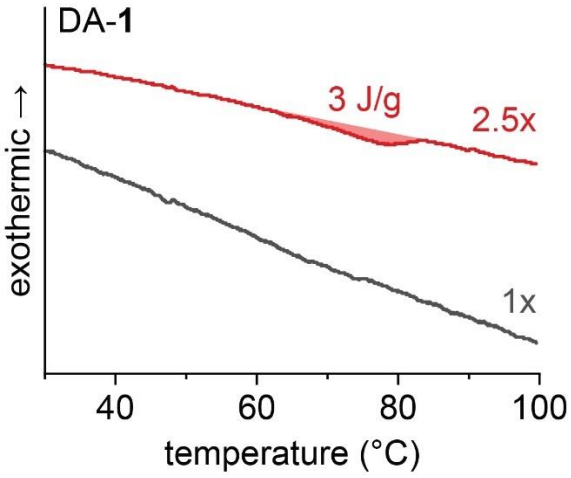

Figure S33. DSC plots of PB-**1**, 0.9 mg (black) and 2.3 mg (red), solvated in 25 μL of toluene.

10. Thermogravimetric analysis (TGA)

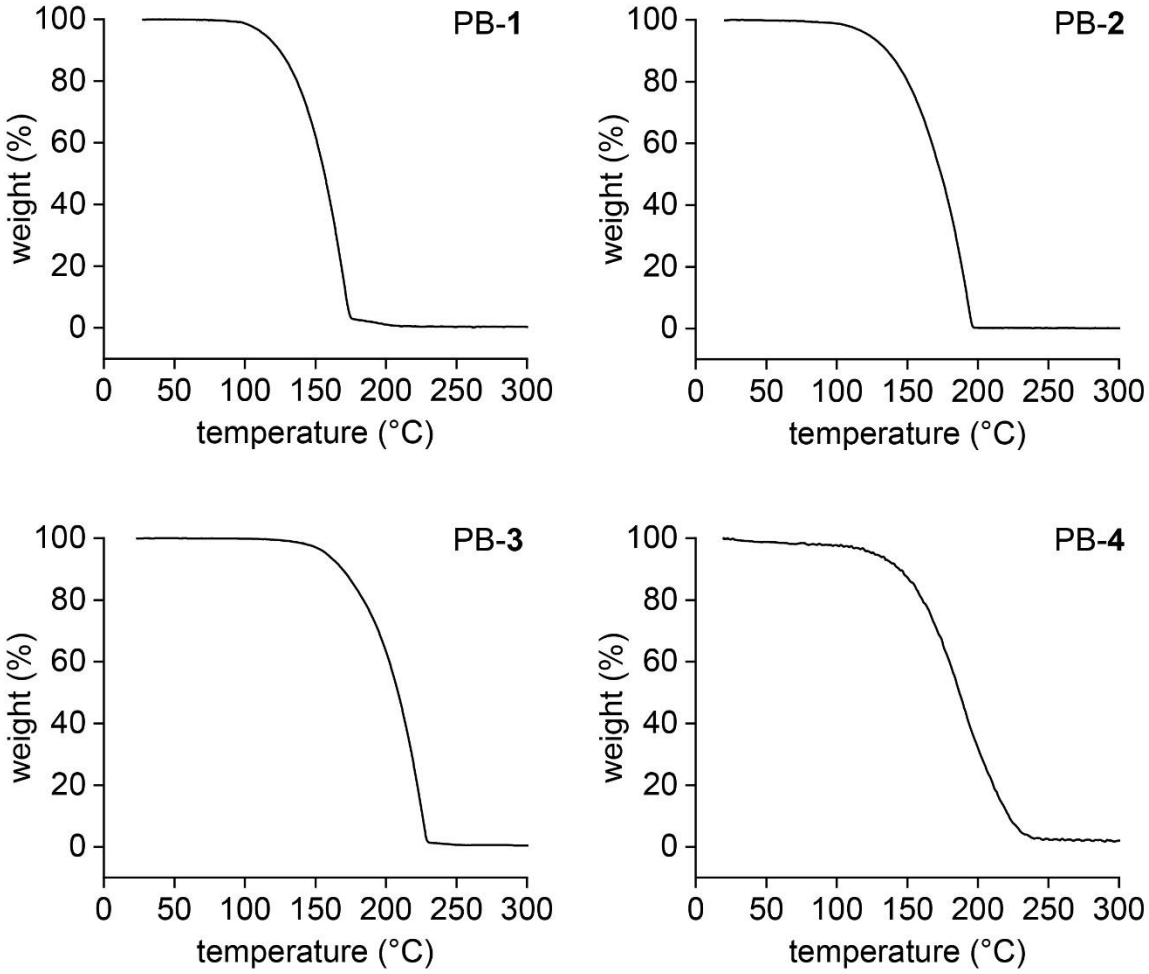

Figure S34. TGA plots for compounds PBs **1**-**4**, measured at a heating rate of 20 °C/min.

11. DSC of dimer in solution

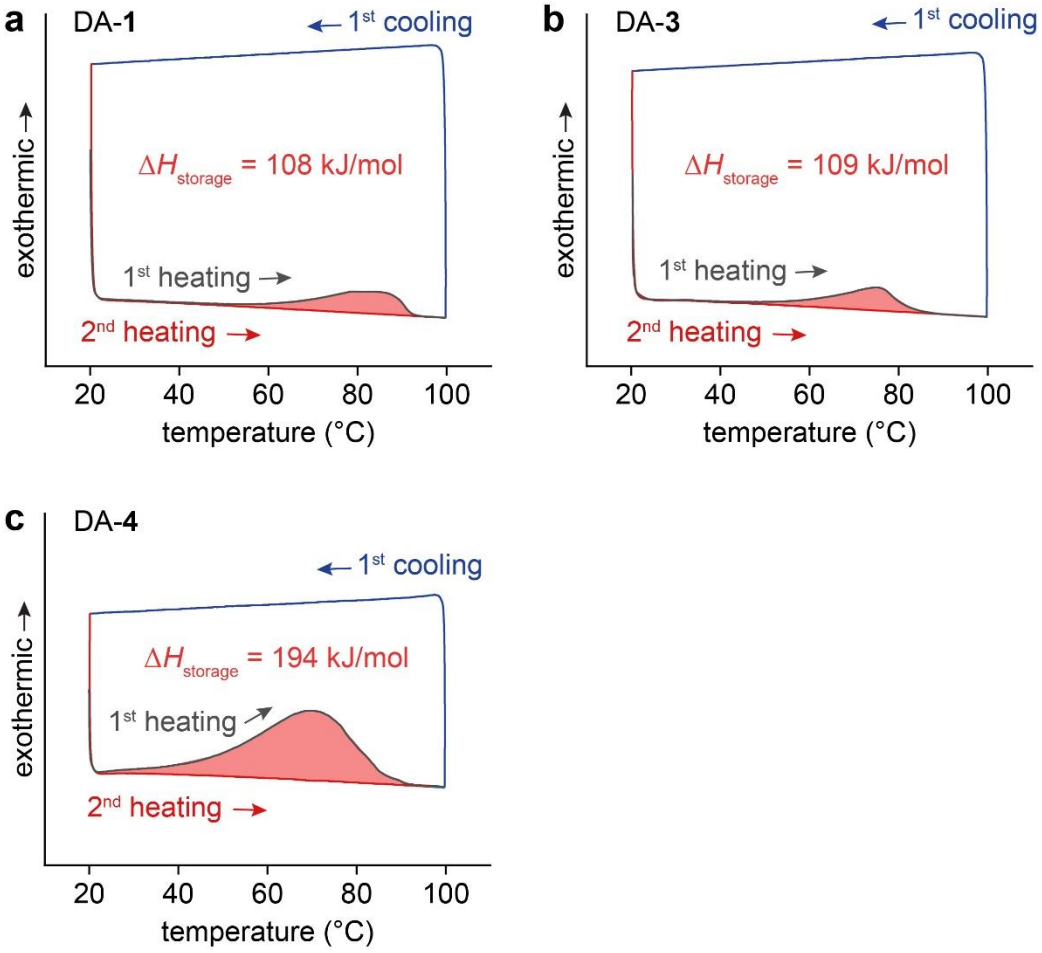

Figure S35. DSC plots of (a) DA-**1**, (b) DA-**3**, and (c) DA-**4** solvated in toluene during the first (black) and second heating (red), and the first cooling (blue) cycle. The highlighted areas are integrated to obtain $\Delta H_{storage}$ values.

12. ^{1}H NMR spectra of dimers after DSC measurement

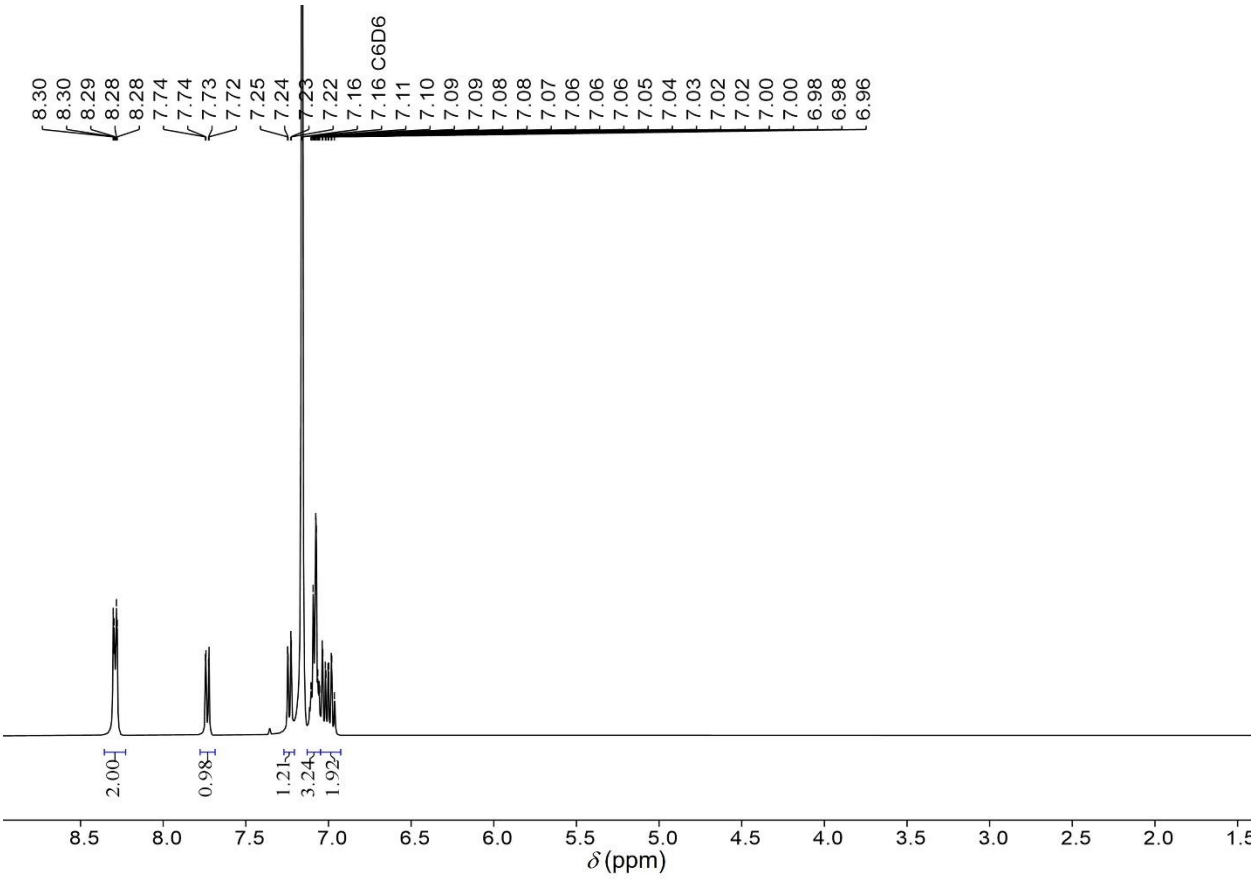

Figure S36. ^{1}H NMR of DA-**1** after DSC measurement, which confirms the DA→2PB thermal reversion.

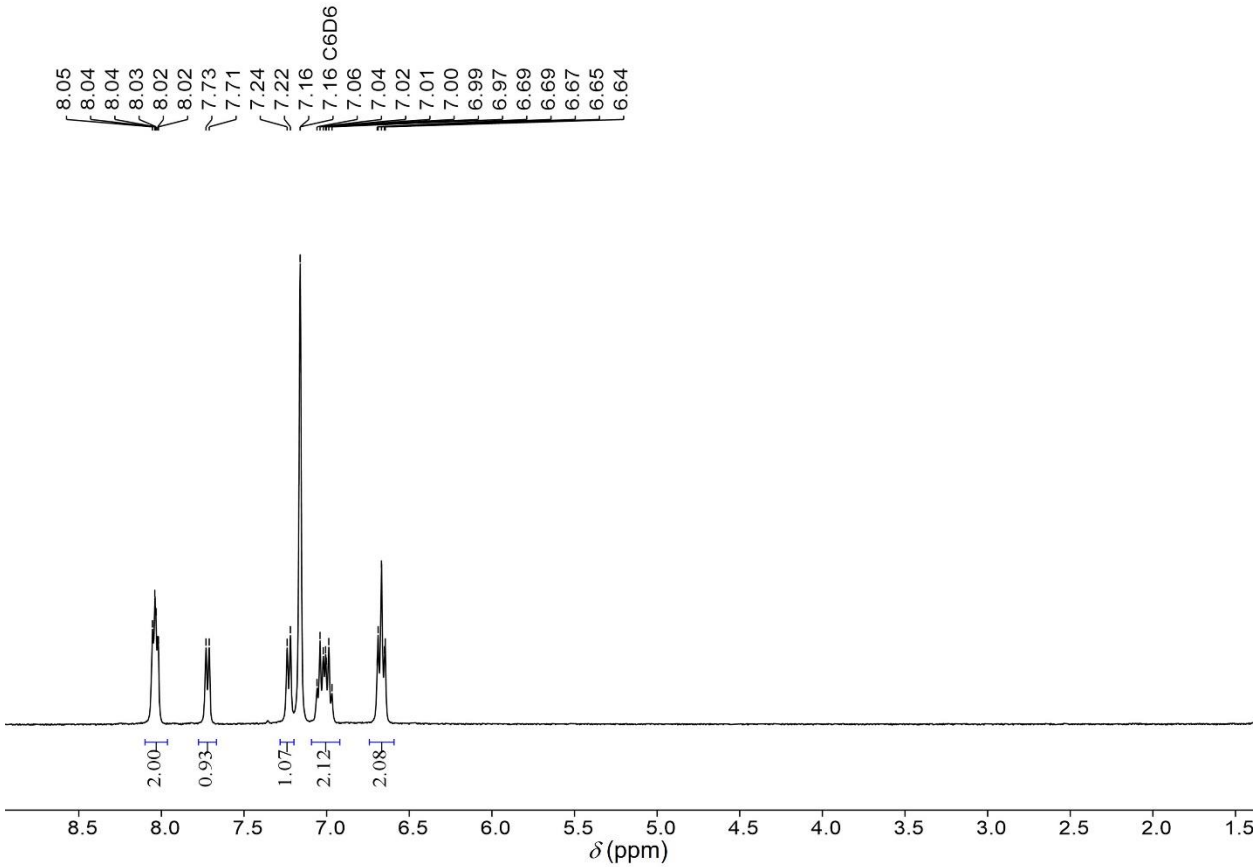

Figure S37. ^{1}H NMR of DA-**2** after DSC measurement, which confirms the DA→2PB thermal reversion.

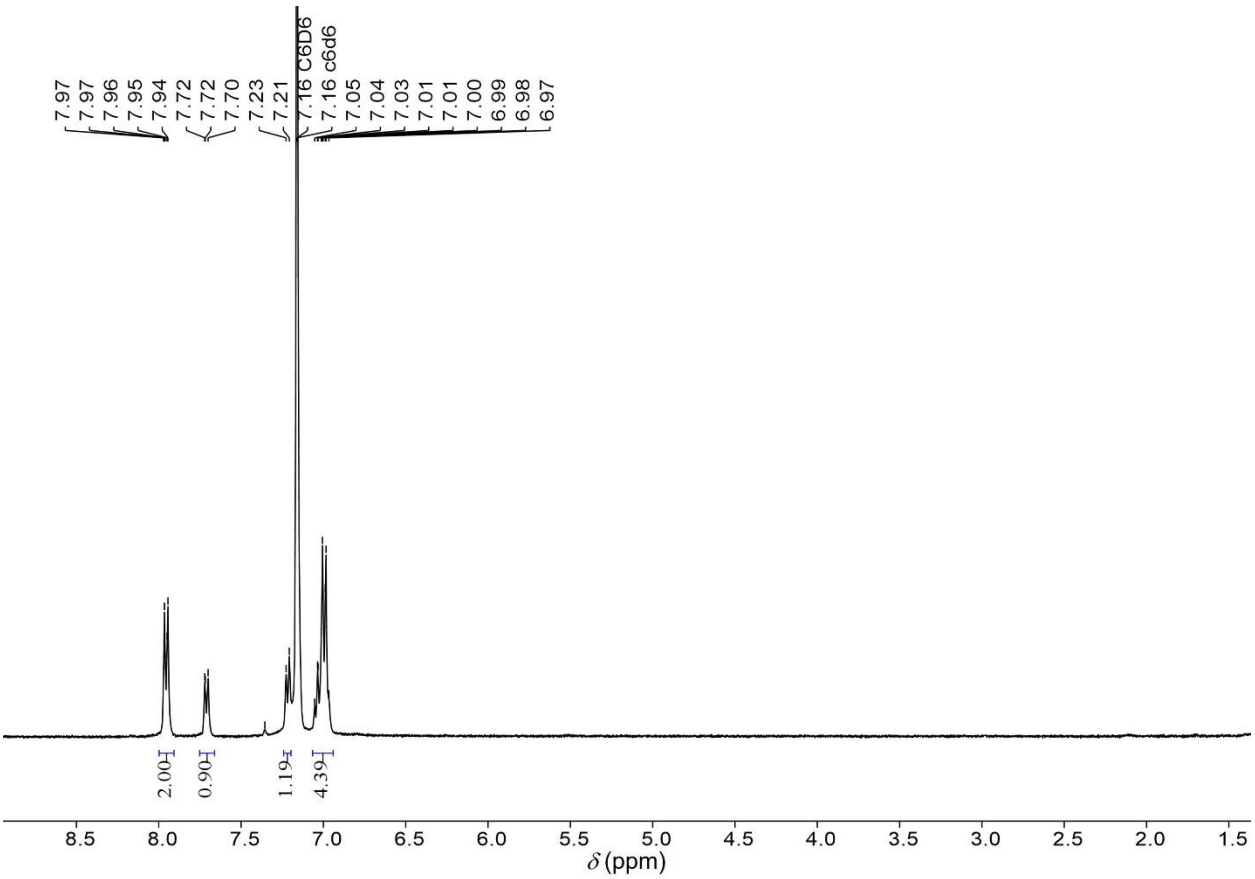

Figure S38. ^{1}H NMR of DA-**3** after DSC measurement, which confirms the DA→2PB thermal reversion.

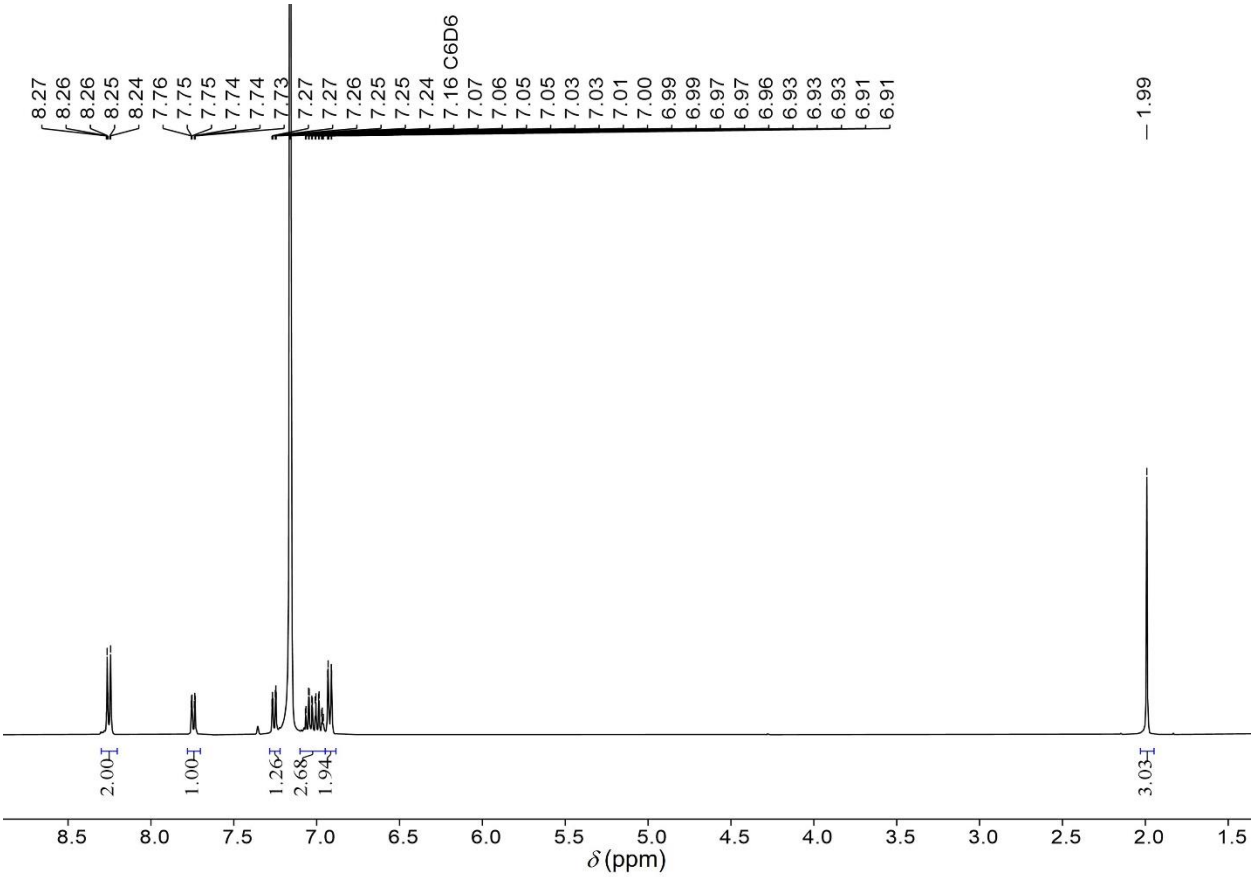

Figure S39. ^{1}H NMR of DA-**4** after DSC measurement, which confirms the DA→2PB thermal reversion.

13. Thermal reversion kinetics measurement in solutions by UV-vis spectroscopy

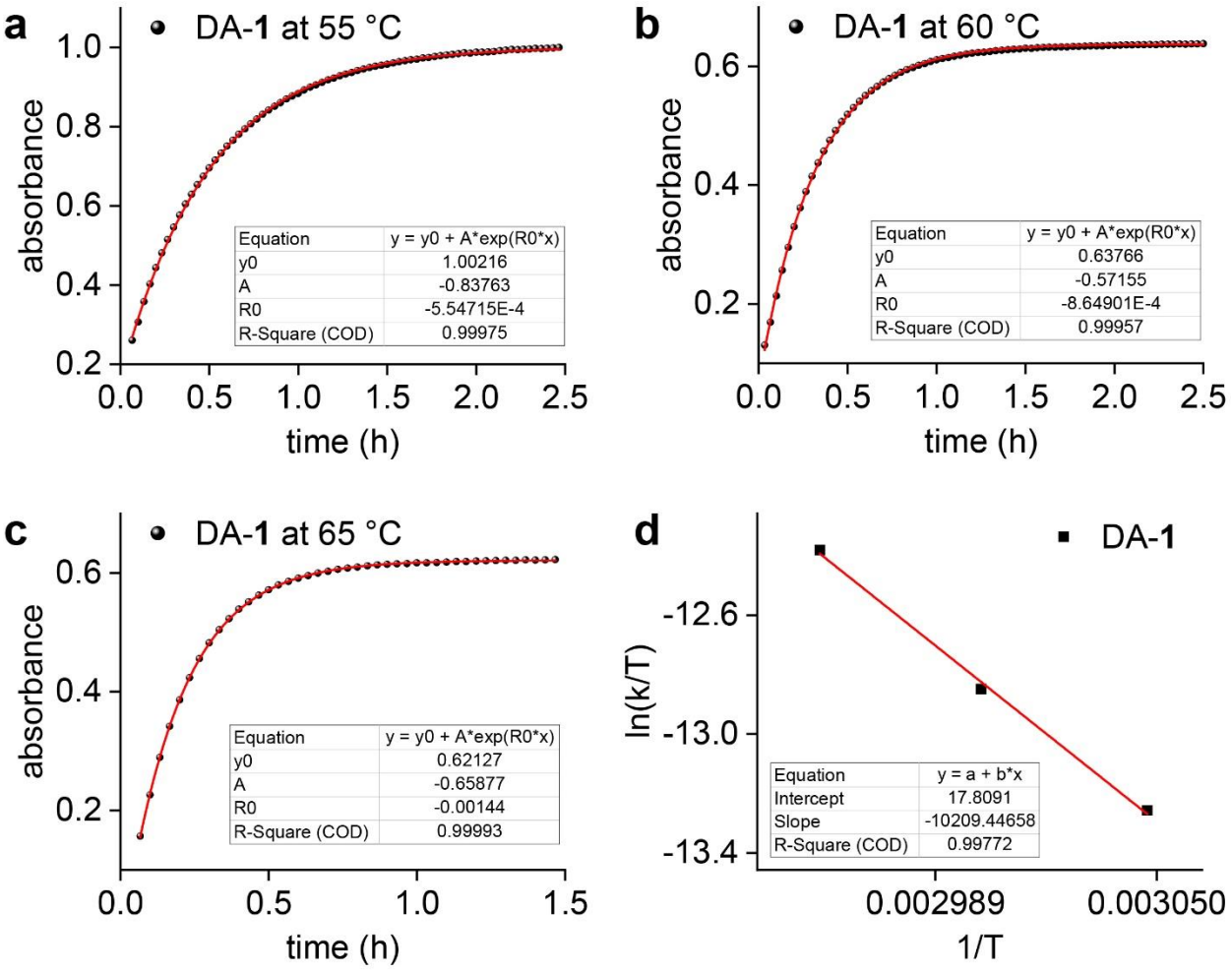

Figure S40. The conversion of DA-**1** at (a) 55 °C, (b) 60 °C, and (c) 65 °C in toluene, and the corresponding (d) Eyring plot. The conversion at each temperature was fitted to an exponential function. The fitted parameters were used to obtain the Eyring plot. The thermal half-life of DA-**1** at 25 °C was determined *via* the extrapolation of the Eyring plot.

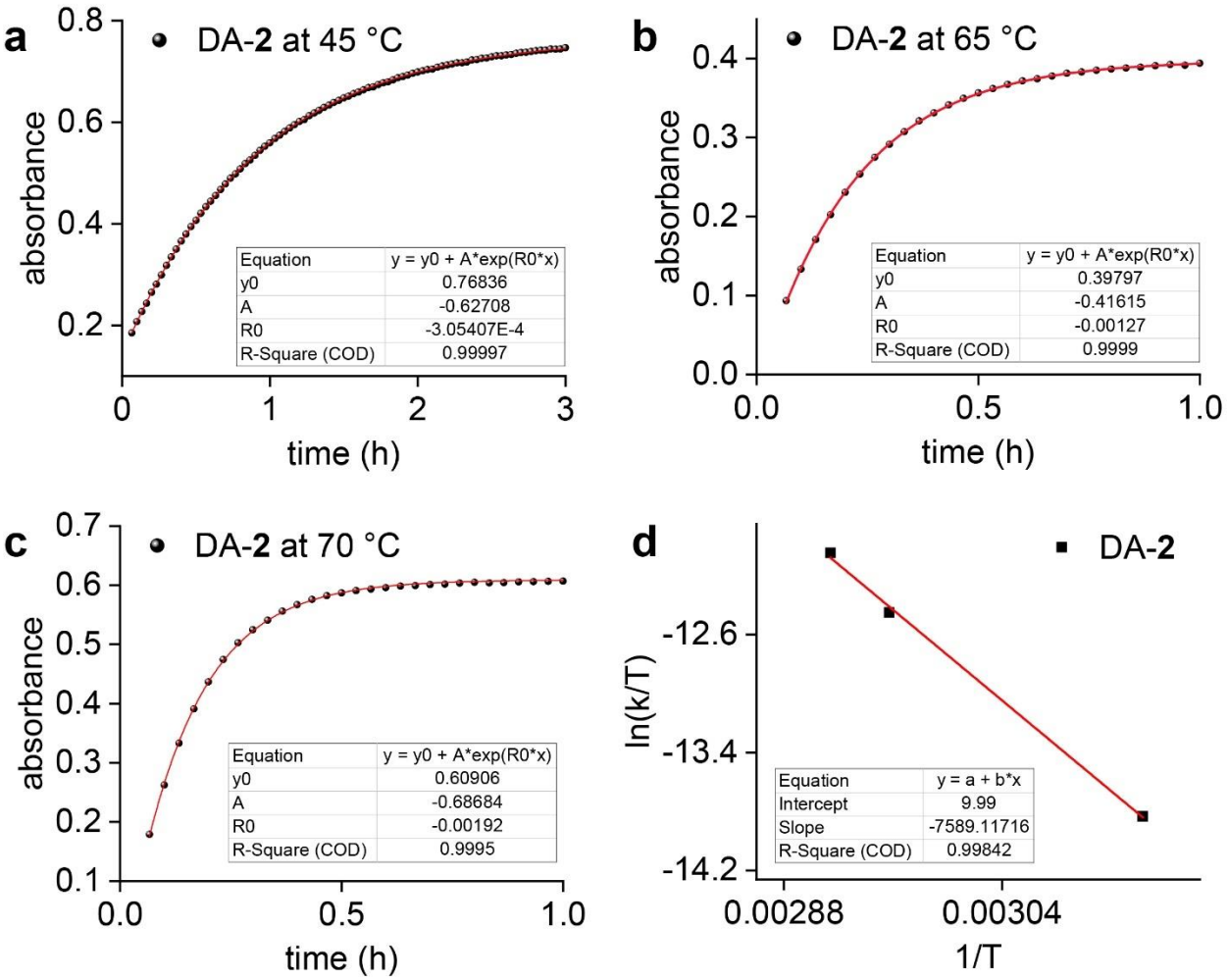

Figure S41. The conversion of DA-**2** at (a) 45 °C, (b) 65 °C, and (c) 70 °C in toluene, and the corresponding (d) Eyring plot. The conversion at each temperature was fitted to an exponential function. The fitted parameters were used to obtain the Eyring plot. The thermal half-life of DA-**2** at 25 °C was determined *via* the extrapolation of the Eyring plot.

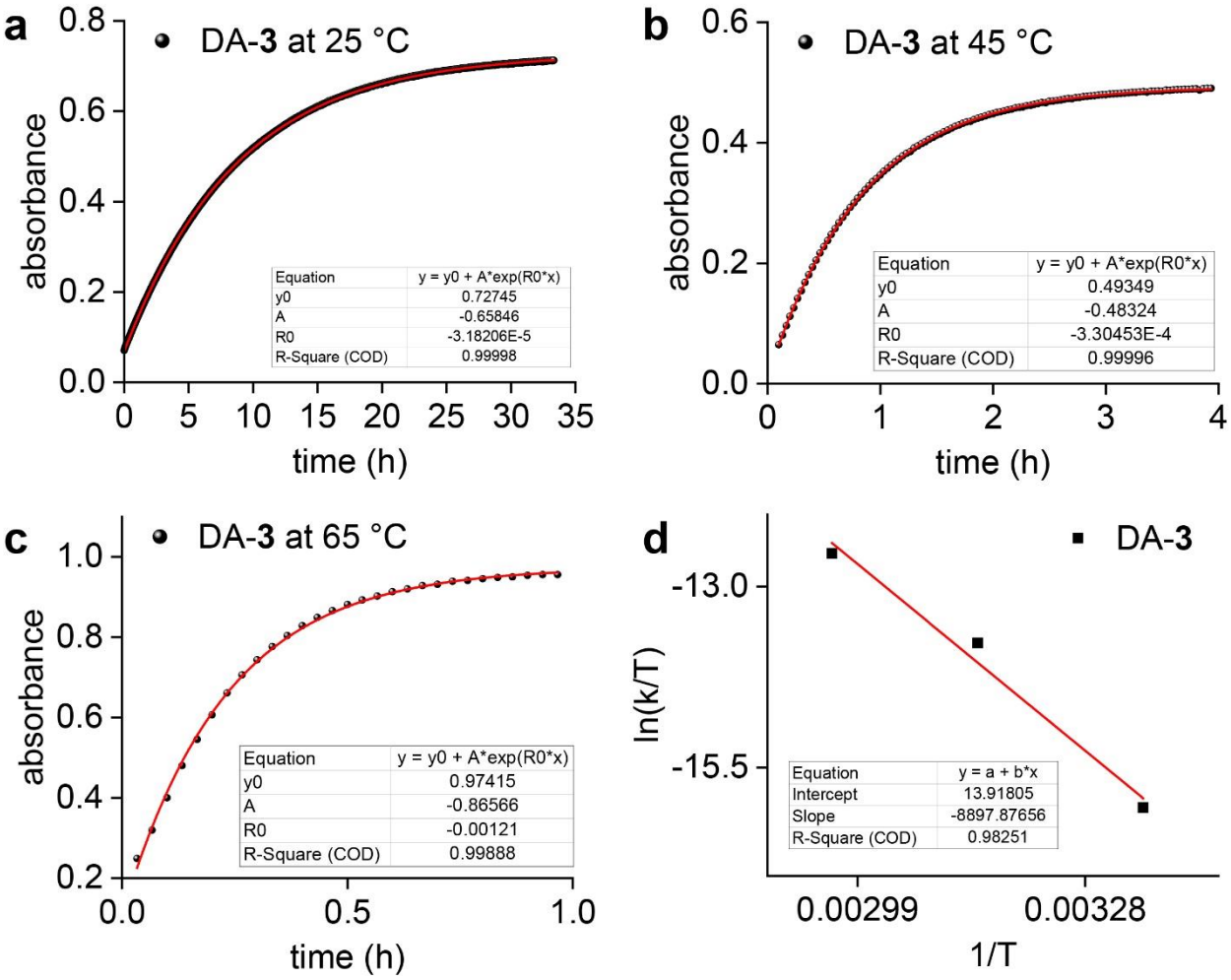

Figure S42. The conversion of DA-**3** at (a) 25 °C, (b) 45 °C, and (c) 65 °C in toluene, and the corresponding (d) Eyring plot. The conversion at each temperature was fitted to an exponential function. The fitted parameters were used to obtain the Eyring plot. The thermal half-life of DA-**3** at 25 °C was determined *via* the extrapolation of the Eyring plot.

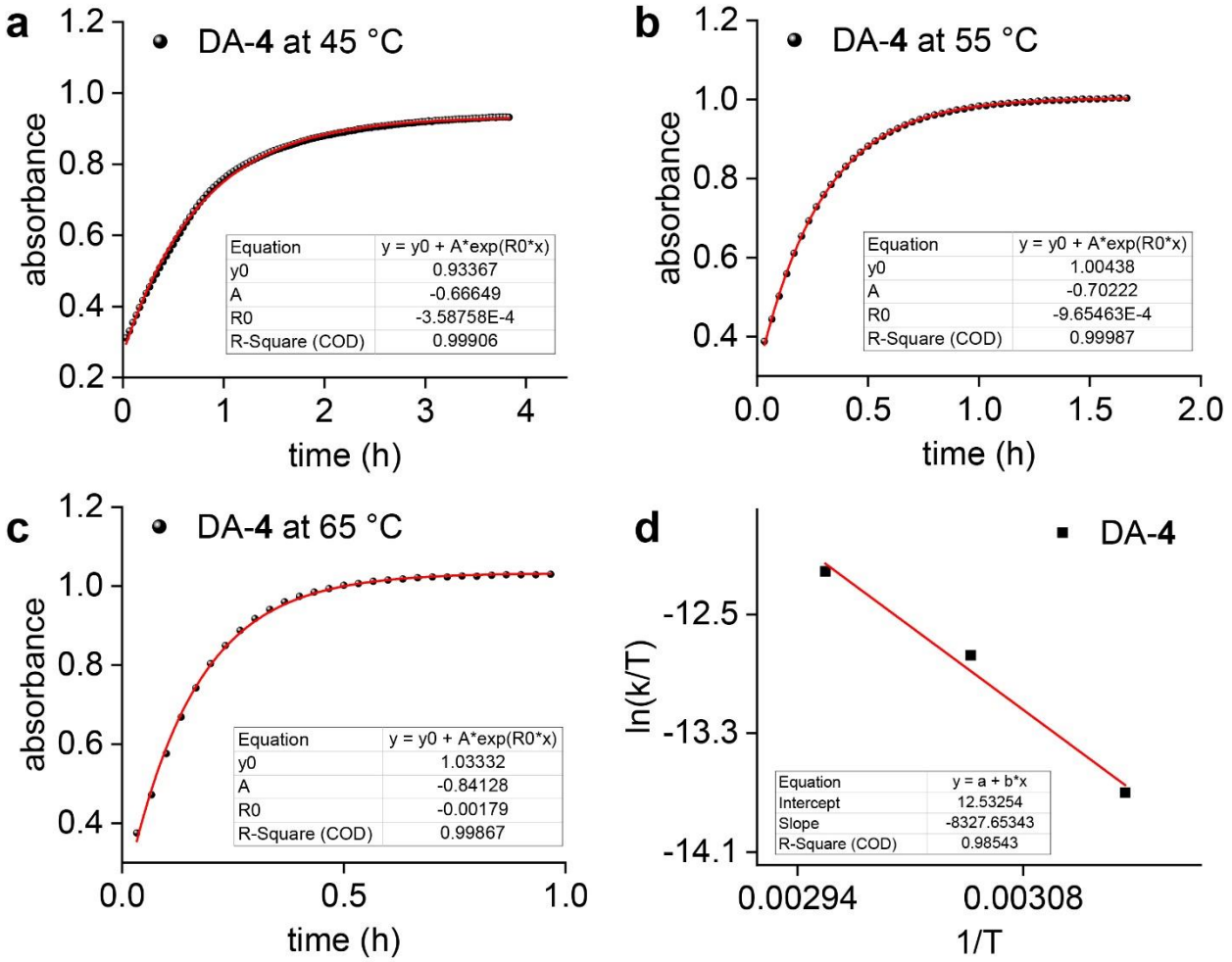

Figure S43. The conversion of DA-**4** at (a) 45 °C, (b) 55 °C, and (c) 65 °C in toluene, and the corresponding (d) Eyring plot. The conversion at each temperature was fitted to an exponential function. The fitted parameters were used to obtain the Eyring plot. The thermal half-life of DA-**4** at 25 °C was determined *via* the extrapolation of the Eyring plot.

14. Computational studies: Thermal cycloreversion

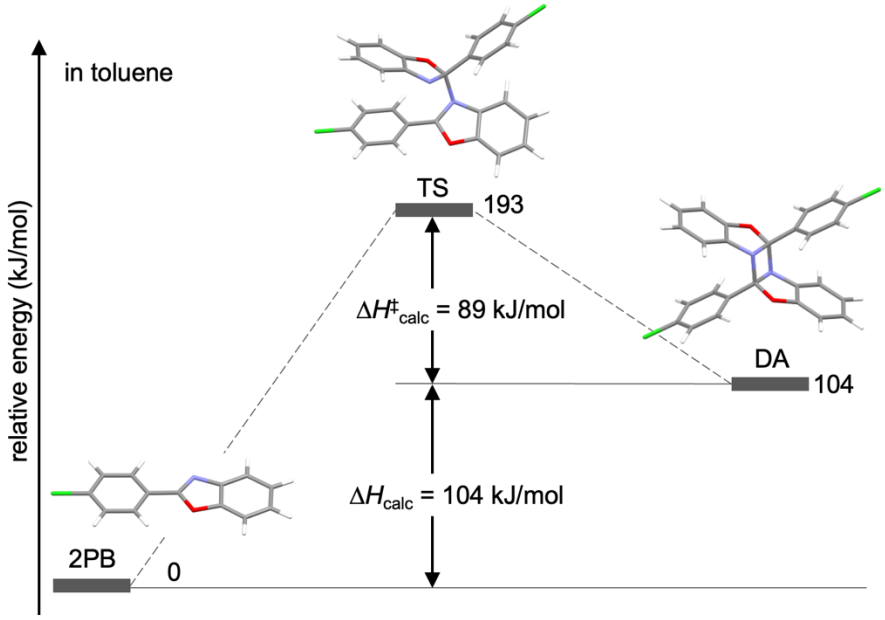

Figure S44. Energy profiles for the thermal reversion of DA-**3** to PB-**3** calculated by DFT calculations and their optimized structures calculated at the B3LYP-D3/6-31+G(d,p) level of theory. Calculations were performed in toluene based on the polarizable continuum model. The energy of the PB form was used as the reference point, set to zero.

Table S2. ΔH_{calc} and $\Delta H^{\ddagger}_{calc}$ in the respective reaction fields estimated by DFT calculations (B3LYP-D3/6-31+G(d,p) level of theory). The calculations were performed based on the polarizable continuum model. The energy of the PB form was used as the reference point, set to zero.

reaction field	ΔH_{calc}	$\Delta H^{\ddagger}_{calc}$
vacuum	101	92
toluene	104	89
CH_3CN	107	86

Table S3. Cartesian coordinates (Å) of the optimized geometry for PB-**3** in toluene.

H	-1.45150	4.42919	-0.00000	O	1.32685	1.01394	0.00000
C	-0.41271	4.11879	-0.00000	C	-0.28249	-0.79837	-0.00000
C	2.33774	3.28635	0.00000	C	-0.86954	-3.51378	-0.00000
C	-0.06849	2.76461	-0.00000	C	-1.61748	-1.23268	-0.00000
C	0.63116	5.04310	0.00000	C	0.75341	-1.74384	0.00000
C	1.97833	4.63695	0.00000	C	0.46316	-3.10438	0.00000
C	1.28377	2.38745	0.00000	C	-1.91549	-2.58931	-0.00000
H	0.40219	6.10378	0.00000	H	-2.41119	-0.49482	-0.00000
H	2.75919	5.39024	0.00000	H	1.78484	-1.41207	0.00000
H	3.37178	2.96235	0.00000	H	1.25903	-3.83956	0.00000
N	-0.85347	1.61204	-0.00000	H	-2.94382	-2.93058	-0.00000
C	0.00000	0.62932	0.00000	Cl	-1.24113	-5.22998	-0.00000

Table S4. Cartesian coordinates (Å) of the optimized geometry for DA-**3** in toluene.

N	0.74253	-0.74984	-0.12753	C	0.61639	0.25780	2.22305
C	-0.58782	-0.45060	-0.73728	C	0.47366	-0.06326	4.97342
C	0.58782	0.45060	0.73728	C	0.90128	1.33297	3.06838
N	-0.74253	0.74984	0.12753	C	0.26309	-0.97977	2.76576
C	2.37953	0.78513	-0.60144	C	0.19193	-1.14846	4.14591
C	1.91349	-0.49833	-0.89946	C	0.83147	1.17834	4.45075
C	-2.37953	-0.78513	0.60144	H	1.18353	2.28964	2.64440
C	-1.91349	0.49833	0.89946	H	0.04914	-1.80877	2.10141
C	3.48981	1.32792	-1.22107	H	-0.07844	-2.10615	4.57446
H	3.83474	2.32708	-0.98200	H	1.05247	2.00630	5.11388
C	4.13500	0.52894	-2.17876	C	-0.61639	-0.25780	-2.22305
H	5.01143	0.91990	-2.68523	C	-0.47366	0.06326	-4.97342
C	3.67252	-0.75065	-2.49005	C	-0.90128	-1.33297	-3.06838
H	4.18865	-1.34188	-3.23875	C	-0.26309	0.97977	-2.76576
C	2.54692	-1.28515	-1.84482	C	-0.19193	1.14846	-4.14591
H	2.17003	-2.27233	-2.08664	C	-0.83147	-1.17834	-4.45075
C	-2.54692	1.28515	1.84482	H	-1.18353	-2.28964	-2.64440
H	-2.17003	2.27233	2.08664	H	-0.04914	1.80877	-2.10141
C	-3.67252	0.75065	2.49005	H	0.07844	2.10615	-4.57446
H	-4.18865	1.34188	3.23875	H	-1.05247	-2.00630	-5.11388
C	-4.13500	-0.52894	2.17876	O	1.58693	1.40541	0.33971
H	-5.01143	-0.91990	2.68523	O	-1.58693	-1.40541	-0.33971
C	-3.48981	-1.32792	1.22107	Cl	0.37995	-0.26548	6.71811
H	-3.83474	-2.32708	0.98200	Cl	-0.37995	0.26548	-6.71811

Table S5. Cartesian coordinates (Å) of the optimized geometry for transition state (thermal reversion of DA-**3** to 2PB-**3**) in toluene.

N	-0.44188	0.98875	-0.58487	C	2.05885	1.23800	-0.09779
C	-0.54728	-0.45013	-0.17141	C	4.74666	0.51565	-0.15740
C	0.66925	1.57771	-0.00393	C	2.94786	1.71423	0.89101
N	0.21288	-0.50611	1.06375	C	2.55115	0.41202	-1.12582
C	-0.97941	3.04562	0.14599	C	3.89623	0.05667	-1.15500
C	-1.49464	1.92904	-0.51168	C	4.28195	1.35217	0.86636
C	1.11608	-1.92654	-0.50016	H	2.57008	2.33984	1.69127
C	1.15206	-1.46089	0.83997	H	1.88440	0.08649	-1.91193
C	-1.70569	4.18454	0.42686	H	4.27178	-0.59122	-1.93686
H	-1.25980	5.03039	0.93580	H	4.96386	1.69802	1.63390
C	-3.04128	4.17518	0.00588	C	-1.99322	-0.89142	-0.05544
H	-3.66333	5.04311	0.19483	C	-4.66653	-1.59892	0.18479
C	-3.57983	3.06718	-0.65816	C	-2.65661	-1.49409	-1.12674
H	-4.61830	3.08927	-0.97092	C	-2.67165	-0.67050	1.14452
C	-2.82043	1.92506	-0.93464	C	-4.01337	-1.01912	1.27148
H	-3.25289	1.07375	-1.44116	C	-3.99924	-1.85028	-1.01354
C	2.18181	-1.92873	1.67547	H	-2.11683	-1.68805	-2.04608
H	2.25471	-1.57040	2.69631	H	-2.12853	-0.23188	1.97373
C	3.10270	-2.83873	1.15461	H	-4.54851	-0.84803	2.19819
H	3.90381	-3.20273	1.79083	H	-4.52268	-2.32035	-1.83803
C	3.01734	-3.30323	-0.16537	O	0.35983	2.81575	0.43689
H	3.73897	-4.02578	-0.53148	O	0.09818	-1.28402	-1.17522
C	2.00440	-2.84226	-1.02280	Cl	6.43303	0.04103	-0.17023
H	1.93264	-3.17064	-2.05418	Cl	-6.36323	-2.03241	0.33069

15. Comparison of reported cycloaddition MOST systems

Table S6. Comparison of reported intramolecular and intermolecular cycloaddition-based MOST energy storage systems.

MOST Systems	Cycloaddition phase(s)	Irradiation wavelength(s)	$t_{1/2}$ of metastable isomer/dimer	Energy storage densities
Norbornadiene/ Quadricyclane[10-12]	solution or neat liquid	236 to 460 nm	10 minutes to 18 years	152-970 J/g
Styrylpyrylium/ Cyclobutane dimerization[13]	crystalline	470 or 530 nm	4 days to 32 years	6-51 J/g
Styryldipyrylium/Cyclobutane polymerization[14]	crystalline or amorphous	470 nm	-	13 J/g
Anthracene/ Dianthracene dimerization[15]	crystalline	365 or 405 nm	1 day to 190 years	195-221 J/g
(This Work) Benzoxazole/ Diazetidine dimerization	biphasic solution	300 nm	135 days to 23 years	224-318 J/g

16. Computational studies: Dearomative cycloaddition

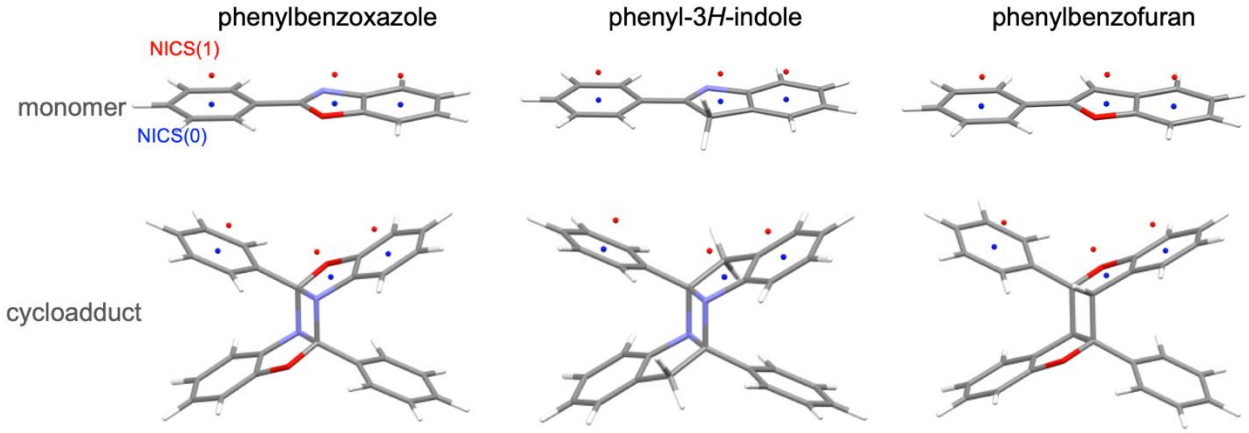

Figure S45. Optimized structures of phenylbenzoxazole, phenyl-3*H*-indole, and phenylbenzofuran and their cycloadducts calculated at the B3LYP-D3/6-31G** level of theory.

Table S7. Cartesian coordinates (Å) of the optimized geometry for phenylbenzoxazole (PB-**1**).

O	0.44030	-0.95430	0.00000	H	0.22810	-3.71060	0.00000
C	0.00000	0.35830	0.00000	C	1.02970	1.38660	0.00000
C	-0.67400	-1.74820	0.00000	C	3.01190	3.37640	0.00000
C	-1.36630	0.40840	0.00000	C	0.67760	2.74750	0.00000
C	-1.83590	-0.95070	0.00000	C	2.39070	1.03850	0.00000
C	-3.08840	-1.58310	0.00000	C	3.37010	2.02800	0.00000
H	-4.00430	-1.00080	0.00000	C	1.66050	3.73060	0.00000
C	-3.12740	-2.97380	0.00000	H	-0.36920	3.03340	0.00000
H	-4.08690	-3.48130	0.00000	H	2.66830	-0.00880	0.00000
C	-1.94750	-3.74040	0.00000	H	4.41790	1.74370	0.00000
H	-2.01560	-4.82350	0.00000	H	1.37210	4.77720	0.00000
C	-0.69080	-3.13550	0.00000	H	-1.97080	1.30280	0.00000

Table S8. Cartesian coordinates (Å) of the optimized geometry for phenylbenzoxazole cycloadduct (DA-**1**).

N	0.63280	-0.75920	-0.38950	C	1.27460	0.09480	1.94000
C	-0.80370	-0.38420	-0.54680	C	1.97290	-0.40400	4.59420
C	0.80370	0.38420	0.54680	C	1.84520	1.10910	2.71380
N	-0.63280	0.75920	0.38950	C	1.05600	-1.16910	2.49320
C	2.12110	0.75570	-1.25300	C	1.40760	-1.41680	3.81840
C	1.52560	-0.49120	-1.46540	C	2.19290	0.85800	4.03970
C	-2.12110	-0.75570	1.25300	H	2.02050	2.08280	2.27040
C	-1.52560	0.49120	1.46540	H	0.61730	-1.94490	1.87610
C	3.02030	1.30310	-2.14910	H	1.24010	-2.40070	4.24510
H	3.46870	2.27350	-1.97080	H	2.63830	1.64610	4.63900
C	3.31030	0.55020	-3.29800	H	2.24510	-0.59810	5.62720
H	4.01420	0.94650	-4.02290	C	-1.27460	-0.09480	-1.94000
C	2.71350	-0.69050	-3.52410	C	-1.97290	0.40400	-4.59420
H	2.95260	-1.24660	-4.42430	C	-1.84520	-1.10910	-2.71380
C	1.80760	-1.23130	-2.59920	C	-1.05600	1.16910	-2.49320
H	1.32560	-2.18720	-2.76890	C	-1.40760	1.41680	-3.81840
C	-1.80760	1.23130	2.59920	C	-2.19290	-0.85800	-4.03970
H	-1.32560	2.18720	2.76890	H	-2.02050	-2.08280	-2.27040
C	-2.71350	0.69050	3.52410	H	-0.61730	1.94490	-1.87610
H	-2.95260	1.24660	4.42430	H	-1.24010	2.40070	-4.24510
C	-3.31030	-0.55020	3.29800	H	-2.63830	-1.64610	-4.63900
H	-4.01420	-0.94650	4.02290	H	-2.24510	0.59810	-5.62720
C	-3.02030	-1.30310	2.14910	O	1.67880	1.33590	-0.08680
H	-3.46870	-2.27350	1.97080	O	-1.67880	-1.33590	0.08680

Table S9. Cartesian coordinates (Å) of the optimized geometry for phenyl-3*H*-indole.

C	-1.38960	-0.34430	0.00000	C	0.24670	1.72890	0.00000
C	0.00000	0.28520	0.00000	C	0.74510	4.49000	0.00000
C	-1.03360	-1.80590	0.00000	C	1.56570	2.21610	0.00000
N	0.96280	-0.58850	0.00000	C	-0.81560	2.64640	0.00000
C	0.37390	-1.87120	0.00000	C	-0.56730	4.01730	0.00000
C	1.04190	-3.09230	0.00000	C	1.80990	3.58390	0.00000
H	2.12600	-3.12450	0.00000	H	2.37820	1.49850	0.00000
C	0.27130	-4.25860	0.00000	H	-1.84030	2.28880	0.00000
H	0.76410	-5.22600	0.00000	H	-1.39820	4.71590	0.00000
C	-1.12610	-4.19860	0.00000	H	2.83260	3.94850	0.00000
H	-1.70210	-5.11870	0.00000	H	0.93860	5.55830	0.00000
C	-1.79280	-2.96520	0.00000	H	-1.96850	-0.04110	0.88100
H	-2.87850	-2.92860	0.00000	H	-1.96850	-0.04110	-0.88100

Table S10. Cartesian coordinates (Å) of the optimized geometry for phenyl-3*H*-indole cycloadduct.

N	0.65950	-0.72270	-0.42860	C	1.34800	0.09250	1.86610
C	-0.83170	-0.44380	-0.49300	C	2.16660	-0.53200	4.47350
C	0.83170	0.44380	0.49300	C	1.66680	1.10970	2.77410
N	-0.65950	0.72270	0.42860	C	1.44520	-1.23870	2.27600
C	1.69190	1.50100	-0.25590	C	1.85750	-1.54950	3.57150
C	-1.69190	-1.50100	0.25590	C	2.06990	0.80100	4.07100
C	2.07970	0.78150	-1.52500	H	1.59080	2.14910	2.46820
C	1.45420	-0.47050	-1.57660	H	1.20790	-2.01800	1.56160
C	-2.07970	-0.78150	1.52500	H	1.93710	-2.58870	3.87610
C	-1.45420	0.47050	1.57660	H	2.30920	1.59960	4.76670
C	2.90880	1.18920	-2.56340	H	2.48370	-0.77440	5.48320
H	3.39830	2.15850	-2.53150	C	-1.34800	-0.09250	-1.86610
C	3.09490	0.34000	-3.65950	C	-2.16660	0.53200	-4.47350
H	3.73790	0.64860	-4.47770	C	-1.66680	-1.10970	-2.77410
C	2.46100	-0.90430	-3.70530	C	-1.44520	1.23870	-2.27600
H	2.61430	-1.55560	-4.56020	C	-1.85750	1.54950	-3.57150
C	1.63810	-1.32610	-2.65850	C	-2.06990	-0.80100	-4.07100
H	1.15020	-2.29390	-2.68290	H	-1.59080	-2.14910	-2.46820
C	-1.63810	1.32610	2.65850	H	-1.20790	2.01800	-1.56160
H	-1.15020	2.29390	2.68290	H	-1.93710	2.58870	-3.87610
C	-2.46100	0.90430	3.70530	H	-2.30920	-1.59960	-4.76670
H	-2.61430	1.55560	4.56020	H	-2.48370	0.77440	-5.48320
C	-3.09490	-0.34000	3.65950	H	-2.56520	-1.79570	-0.33170
H	-3.73790	-0.64860	4.47770	H	-1.09750	-2.39950	0.45430
C	-2.90880	-1.18920	2.56340	H	1.09750	2.39950	-0.45430
H	-3.39830	-2.15850	2.53150				

Table S11. Cartesian coordinates (Å) of the optimized geometry for phenylbenzofuran.

O	0.44030	-0.95430	0.00000	C	1.02970	1.38660	0.00000
C	0.00000	0.35830	0.00000	C	3.01190	3.37640	0.00000
C	-0.67400	-1.74820	0.00000	C	0.67760	2.74750	0.00000
C	-1.36630	0.40840	0.00000	C	2.39070	1.03850	0.00000
C	-1.83590	-0.95070	0.00000	C	3.37010	2.02800	0.00000
C	-3.08840	-1.58310	0.00000	C	1.66050	3.73060	0.00000
H	-4.00430	-1.00080	0.00000	H	-0.36920	3.03340	0.00000
C	-3.12740	-2.97380	0.00000	H	2.66830	-0.00880	0.00000
H	-4.08690	-3.48130	0.00000	H	4.41790	1.74370	0.00000
C	-1.94750	-3.74040	0.00000	H	1.37210	4.77720	0.00000
H	-2.01560	-4.82350	0.00000	H	-1.97080	1.30280	0.00000
C	-0.69080	-3.13550	0.00000	H	3.77750	4.14580	0.00000
H	0.22810	-3.71060	0.00000				

Table S12. Cartesian coordinates (Å) of the optimized geometry for phenylbenzofuran cycloadduct.

C	0.62730	-0.81250	-0.41930	H	-3.50070	-2.30940	1.90060
C	-0.87010	-0.35980	-0.59270	C	1.37480	0.08190	1.97910
C	0.87010	0.35980	0.59270	C	2.21680	-0.37820	4.61540
C	-0.62730	0.81250	0.41930	C	2.24620	0.97530	2.61080
O	1.74890	1.30170	-0.07990	C	0.93080	-1.04570	2.68090
O	-1.74890	-1.30170	0.07990	C	1.34760	-1.27290	3.99040
C	2.16350	0.74460	-1.26060	C	2.66580	0.74450	3.92050
C	1.57300	-0.49190	-1.53190	H	2.59770	1.84270	2.06540
C	-2.16350	-0.74460	1.26060	H	0.24900	-1.74530	2.21040
C	-1.57300	0.49190	1.53190	H	0.99240	-2.15060	4.52140
C	3.05680	1.34860	-2.13490	H	3.34640	1.44370	4.39700
H	3.50070	2.30940	-1.90060	H	2.54310	-0.55660	5.63550
C	3.35120	0.66680	-3.32120	C	-1.37480	-0.08190	-1.97910
H	4.04700	1.11140	-4.02620	C	-2.21680	0.37820	-4.61540
C	2.76860	-0.56920	-3.61300	C	-2.24620	-0.97530	-2.61080
H	3.01020	-1.07410	-4.54230	C	-0.93080	1.04570	-2.68090
C	1.86880	-1.15500	-2.71520	C	-1.34760	1.27290	-3.99040
H	1.39660	-2.10490	-2.94530	C	-2.66580	-0.74450	-3.92050
C	-1.86880	1.15500	2.71520	H	-2.59770	-1.84270	-2.06540
H	-1.39660	2.10490	2.94530	H	-0.24900	1.74530	-2.21040
C	-2.76860	0.56920	3.61300	H	-0.99240	2.15060	-4.52140
H	-3.01020	1.07410	4.54230	H	-3.34640	-1.44370	-4.39700
C	-3.35120	-0.66680	3.32120	H	-2.54310	0.55660	-5.63550
H	-4.04700	-1.11140	4.02620	H	0.70060	-1.82900	-0.02890
C	-3.05680	-1.34860	2.13490	H	-0.70060	1.82900	0.02890

C	-5.231170	-0.034670	-0.048970	H	-1.117640	-2.942640	0.927440
C	-2.980760	0.284580	-0.949780	C	0.121640	-4.552410	0.340350
H	-2.360920	0.557030	-1.800490	O	11.828510	0.136300	0.654730
C	-4.364170	0.317220	-1.104760	C	5.242610	0.010880	0.119420
H	-4.781830	0.609670	-2.063780	C	2.926170	-0.276610	0.846110
C	-6.675130	-0.008090	-0.292240	H	2.239450	-0.556820	1.641320
H	-6.950070	0.299060	-1.298920	C	9.115020	0.208120	0.053750
C	-7.659170	-0.327020	0.586170	C	4.293470	-0.350300	1.098690
H	-7.402710	-0.634500	1.595860	H	4.633670	-0.681910	2.075410
O	1.135790	-4.982940	-0.405460	C	10.104860	0.581780	-0.891980
C	-2.400480	-0.106930	0.268150	H	9.836690	0.911370	-1.889360
C	-4.647200	-0.405440	1.179150	C	11.431340	0.532150	-0.556230
H	-5.267350	-0.681440	2.025100	C	6.664120	-0.057900	0.464510
C	0.402750	-2.318520	-0.515090	H	6.859350	-0.409000	1.475430
C	-3.264200	-0.439500	1.329150	C	7.715170	0.273470	-0.327570
H	-2.850710	-0.741490	2.288420	H	7.538170	0.626890	-1.339250
C	1.474240	-2.821590	-1.286400	C	9.588950	-0.204880	1.326980
H	2.043830	-2.187520	-1.954620	H	8.923840	-0.508630	2.125320
C	1.802360	-4.151920	-1.206400	C	10.933210	-0.224400	1.578530
C	-0.901690	-0.220870	0.465270	O	-1.240570	5.062610	-0.080690
H	-0.727340	-0.708640	1.428420	C	2.445420	0.165710	-0.397450
C	-0.052910	-0.893810	-0.662020	C	4.758090	0.431720	-1.135340
H	-0.612430	-0.884430	-1.606870	H	5.444200	0.715590	-1.925920
C	-0.272760	-3.235870	0.316320	C	-0.418170	2.431900	0.163600

17. References

1. P. Lentes, P. Frühwirt, H. Freißmuth, W. Moormann, F. Kruse, G. Gescheidt and R. Herges, Photoswitching of Diazocines in Aqueous Media, *J. Org. Chem.*, 2021, **86**, 4355-4360.
2. M. J. Frisch, G. W. Trucks, H. B. Schlegel, G. E. Scuseria, M. A. Robb, J. R. Cheeseman, G. Scalmani, V. Barone, G. A. Petersson, H. Nakatsuji, X. Li, M. Caricato, A. V. Marenich, J. Bloino, B. G. Janesko, R. Gomperts, B. Mennucci, H. P. Hratchian, J. V. Ortiz, A. F. Izmaylov, J. L. Sonnenberg, Williams, F. Ding, F. Lipparini, F. Egidi, J. Goings, B. Peng, A. Petrone, T. Henderson, D. Ranasinghe, V. G. Zakrzewski, J. Gao, N. Rega, G. Zheng, W. Liang, M. Hada, M. Ehara, K. Toyota, R. Fukuda, J. Hasegawa, M. Ishida, T. Nakajima, Y. Honda, O. Kitao, H. Nakai, T. Vreven, K. Throssell, J. A. Montgomery Jr., J. E. Peralta, F. Ogliaro, M. J. Bearpark, J. J. Heyd, E. N. Brothers, K. N. Kudin, V. N. Staroverov, T. A. Keith, R. Kobayashi, J. Normand, K. Raghavachari, A. P. Rendell, J. C. Burant, S. S. Iyengar, J. Tomasi, M. Cossi, J. M. Millam, M. Klene, C. Adamo, R. Cammi, J. W. Ochterski, R. L. Martin, K. Morokuma, O. Farkas, J. B. Foresman and D. J. Fox, Gaussian 16 Rev. B.01, 2016.
3. S. Grimme, S. Ehrlich and L. Goerigk, Effect of the damping function in dispersion corrected density functional theory, *J. Comput. Chem.*, 2011, **32**, 1456-1465.
4. P. v. R. Schleyer, C. Maerker, A. Dransfeld, H. Jiao and N. J. R. van Eikema Hommes, Nucleus-Independent Chemical Shifts: A Simple and Efficient Aromaticity Probe, *J. Am. Chem. Soc.*, 1996, **118**, 6317-6318.
5. Z. Chen, C. S. Wannere, C. Corminboeuf, R. Puchta and P. v. R. Schleyer, Nucleus-Independent Chemical Shifts (NICS) as an Aromaticity Criterion, *Chem. Rev.*, 2005, **105**, 3842-3888.

6. A. Ghodbane, S. D'Altério, N. Saffon, N. D. McClenaghan, L. Scarpantonio, P. Jolinat and S. Fery-Forgues, Facile Access to Highly Fluorescent Nanofibers and Microcrystals via Reprecipitation of 2-Phenyl-benzoxazole Derivatives, *Langmuir*, 2012, **28**, 855-863.

7. A. Ghodbane, N. Saffon, S. Blanc and S. Fery-Forgues, Influence of the halogen atom on the solid-state fluorescence properties of 2-phenyl-benzoxazole derivatives, *Dyes Pigm.*, 2015, **113**, 219-226.

8. D. Kim, K. Yoo, S. E. Kim, H. J. Cho, J. Lee, Y. Kim and M. Kim, Copper-Catalyzed Selective Arylations of Benzoxazoles with Aryl Iodides, *J. Org. Chem.*, 2015, **80**, 3670-3676.

9. N. Paillous, S. F. Forgues, J. Jaud and J. Devillers, [2 + 2] Cycloaddition of two C=N double bonds. First structural evidence for head-to-tail photodimerization in the 2-phenylbenzoxazole series, *J. Chem. Soc., Chem. Commun.*, 1987, 578-579.

10. C.-L. Sun, C. Wang and R. Boulatov, Applications of Photoswitches in the Storage of Solar Energy, *ChemPhotoChem*, 2019, **3**, 268-283.

11. R. J. Salthouse and K. Moth-Poulsen, Multichromophoric photoswitches for solar energy storage: from azobenzene to norbornadiene, and MOST things in between, *J. Mater. Chem. A*, 2024, **12**, 3180-3208.

12. A. Dreos, Z. Wang, J. Udmark, A. Ström, P. Erhart, K. Börjesson, M. B. Nielsen and K. Moth-Poulsen, Liquid Norbornadiene Photoswitches for Solar Energy Storage, *Adv. Energy Mater.*, 2018, **8**, 1703401.

13. S. Cho, J. Usuba, S. Chakraborty, X. Li and G. G. D. Han, Solid-state photon energy storage via reversible [2+2] cycloaddition of donor-acceptor styrylpyrylium system, *Chem*, 2023, **9**, 3159-3171.

14. J. Usuba, Z. Sun, H. P. Q. Nguyen, C. Raju, K. Schmidt-Rohr and G. G. D. Han, Mechanoactivated amorphization and photopolymerization of styryldipyryliums, *Commun. Mater.*, 2024, **5**, 98.

15. S. Chakraborty, H. P. Q. Nguyen, J. Usuba, J. Y. Choi, Z. Sun, C. Raju, G. Sigelmann, Q. Qiu, S. Cho, S. M. Tenney, K. E. Shulenberger, K. Schmidt-Rohr, J. Park and G. G. D. Han, Self-activated energy release cascade from anthracene-based solid-state molecular solar thermal energy storage systems, *Chem*, 2024, DOI: 10.1016/j.chempr.2024.06.033.